



Memo version 1.0

BESIII Analysis Memo

DocDB-497

BAM-228

August 4, 2022

Measurement of decay parameters $\alpha_0/\bar{\alpha}_0$ of $\Lambda/\bar{\Lambda}$ in the process $J/\psi \rightarrow \Xi^-\bar{\Xi}^+$

Liang Liu 1^{a,b}, author 2^a, and author 3^b

^a*Institute of High Energy Physics, CAS*

^b*affil 1*

^c*Department of Computer Science and Engineering*

Internal Referee Committee

Ref1 xx (Chair)^d, Ref2 xx^e, and Ref3 xx^f

^d*Department of Computer Science and Engineering*

^e*Department of Electrical Engineering*

^f*Latex Univeristy*

DocDB : <http://docbes3.ihep.ac.cn/cgi-bin/DocDB>ShowDocument?docid=497>

Hypernews : <http://hnbes3.ihep.ac.cn/HyperNews/get/paper228.html>

Abstract

Based on 567 pb^{-1} of e^+e^- annihilation data collected with the BESIII detector at the BEPCII produced at $\sqrt{s} = 4.599 \text{ GeV}$,

.

.

.

.

.

.

.

.

26 .
27 .
28 .
29 .
30 .
31 .
32 .

1 Contents

2	1 Introduction	3
3	1.1 Previous results	5
4	2 Data Sample	7
5	2.1 BESIII Detector	7
6	2.2 Data sample	7
7	2.3 Monte Carlo Simulation	8
8	2.3.1 Inclusive Monte Carlo	8
9	2.3.2 Signal Monte Carlo	8
10	3 Event Selection	12
11	3.1 Quick review	12
12	3.2 Track level selection	12
13	3.3 Event level selection	13
14	3.4 Further selection	14
15	4 Background estimation	17
16	4.1 Inclusive MC	17
17	4.2 Miscombination background	18
18	5 Parameters estimation	22
19	5.1 Maximum likelihood fit	22
20	5.2 Input-Output check	23
21	6 Real data	24
22	6.1 Blind analysis	24
23	6.2 Signal yield	24
24	6.3 Variables comparison	24
25	6.4 Transverse momentum and polar angle	26
26	6.5 Polarization and entanglement	27
27	6.6 Data fit results	27
28	7 Systematic uncertainty	29
29	8 Summary	30

1	Appendices	33
2	A True information	34
3	B Branch fraction check	42
4	C Comparison between data and MC	43
5	C.1 Variables comparison	43
6	C.2 Transverse momentum and polar angle	43

1 Introduction

From the fundamental point of view, all matter is built out of fermions (spin-1/2 particles) with quarks being the elementary constituents. The antimatter in the modern theory was first predicted by Paul Dirac and discovered by Carl D. Anderson. Cosmological observations tell us that our universe contains more matter than antimatter. The asymmetry between matter and antimatter can be characterized in terms of the baryon-to-photon ratio

$$\eta \equiv \frac{n_B - n_{\bar{B}}}{n_\gamma} \approx 6 \times 10^{-10}. \quad (1)$$

The physical process responsible for the asymmetry is called baryogenesis. To discover the mechanism behind baryogenesis is one of the most important unresolved problems in fundamental physics. For now, it is well known that there necessary conditions for baryogenesis which is called Sakharov's conditions.

1. B violation

2. Loss of thermal equilibrium

3. C, CP violation

In 1956, the idea of testing the violation of parity (P) symmetry was proposed by Tsung-Dao Lee and Chen-Ning Yang firstly. The product of two transformations charge conjugation (C) and parity (P) is the true symmetry between matter and antimatter. The Kobayashi-Maskawa mechanism is the only confirmed way of CP violation predicted by the Standard Model. The measurement of the meson decays show that the Kobayashi-Maskawa is, very likely, the dominant source of CP violation in low-energy flavor-changing processes. However, it predicts present baryon number density that is many orders of magnitude below the cosmological observations, which indicates that there must exist sources of CP violation beyond the Kobayashi-Maskawa phase in our Universe.

The hadronic decay of hyperons proceeds into both parity-violating (*S*-wave) and parity-conserving (*P*-wave) final states with amplitudes *S* and *P*. The amplitude can be written as

$$\text{Amp}(B \rightarrow b\pi) = S + P\sigma \cdot \mathbf{q} \quad (2)$$

The experimental observables are the total decay width Γ , and the normalized decay asymmetry parameters α , β , and γ .

$$\begin{aligned} \alpha^2 + \beta^2 + \gamma^2 &= 1, \\ \alpha &= 2\text{Re}(S^*P)/(|S|^2 + |P|^2), \\ \beta &= 2\text{Im}(S^*P)/(|S|^2 + |P|^2). \end{aligned} \quad (3)$$

- ¹ Only two of these three parameters are independent. So, the decay parameters are usually parametrized
² by using two essentially independent parameters α and ϕ

$$\begin{aligned}\beta &= \sqrt{1 - \alpha^2} \sin \phi, \\ \gamma &= \sqrt{1 - \alpha^2} \cos \phi,\end{aligned}\tag{4}$$

- ³ which are more closely related to experimental measurement. Using α and ϕ , two CP violation observables $A_{CP} = \frac{\alpha + \bar{\alpha}}{\alpha - \bar{\alpha}}$ and $\phi_{CP} = \frac{\phi + \bar{\phi}}{2}$ can be defined. If CP conservation holds, A_{CP} and ϕ_{CP} will be strictly equal to 0. Any nonzero value of A_{CP} and ϕ_{CP} indicates the CP violation in hyperon decay.

In this work, we will focus on the following two decay channel,

$$e^+ e^- \rightarrow J/\psi \rightarrow \Xi^- \bar{\Xi}^+ \rightarrow \Lambda(\rightarrow n\pi^0)\pi^- \bar{\Lambda}(\rightarrow \bar{p}^-\pi^+)\pi^+, \text{(neutron channel)}\tag{5a}$$

$$e^+ e^- \rightarrow J/\psi \rightarrow \Xi^- \bar{\Xi}^+ \rightarrow \Lambda(\rightarrow p^+\pi^-)\pi^- \bar{\Lambda}(\rightarrow \bar{n}\pi^0)\pi^+. \text{(anti-neutron channel)}\tag{5b}$$

- ⁶ Figure 1 shows the diagram of the decay channels. The hadronic decays of two hyperons Ξ^- ($S = 2$) and
⁷ Λ ($S = 1$) will be studied. There are total 10 parameters in this process, two production parameter $\alpha_{J/\psi}$
⁸ and $\Delta\Phi$, four decay asymmetry parameters of Ξ^- , α^Ξ , ϕ^Ξ , $\bar{\alpha}^\Xi$, and $\bar{\phi}^\Xi$, four decay asymmetry parameters
⁹ of Λ , α_\perp^Λ , $\bar{\alpha}_+^\Lambda$, α_0^Λ , and $\bar{\alpha}_0^\Lambda$. The unique advantage of this work is that we can measure the four decay
¹⁰ modes of Λ decay simultaneously,

$$\begin{aligned}\Lambda &\rightarrow p\pi^-, \\ \Lambda &\rightarrow n\pi^0, \\ \bar{\Lambda} &\rightarrow \bar{p}\pi^+, \\ \bar{\Lambda} &\rightarrow \bar{n}\pi^0,\end{aligned}\tag{6}$$

- ¹¹ so that, the isospin amplitude can be studied by combining the four decay modes. For $\Lambda \rightarrow p\pi^-$, the
¹² S-wave and P-wave can be expressed as

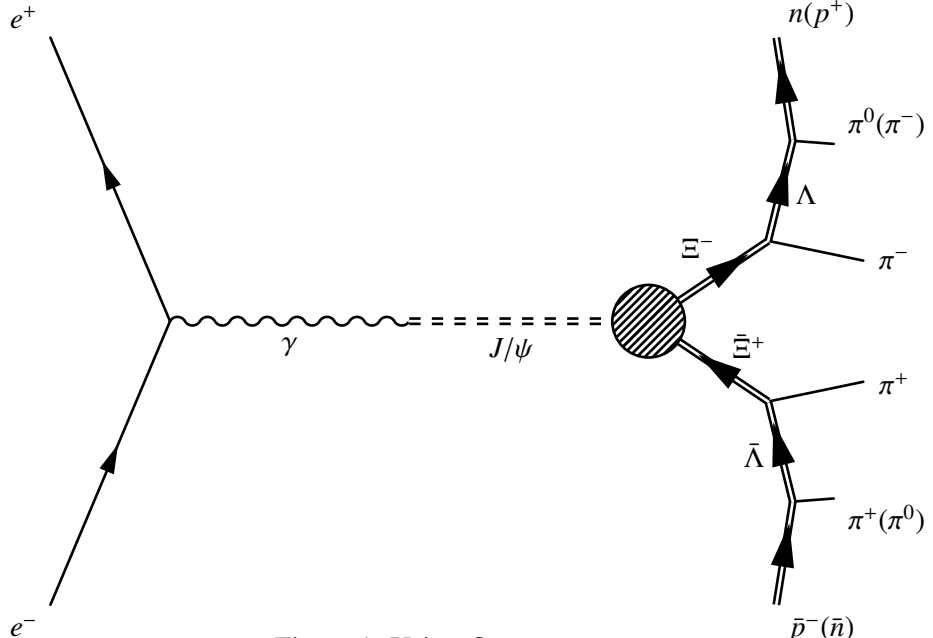
$$\begin{aligned}S(\Lambda_-) &= -\sqrt{\frac{2}{3}}S_{11}e^{i(\delta_{11}^S + \phi_1^S)} + \sqrt{\frac{1}{3}}S_{33}e^{i(\delta_{33}^S + \phi_3^S)}, \\ P(\Lambda_-) &= -\sqrt{\frac{2}{3}}P_{11}e^{i(\delta_{11}^P + \phi_1^P)} + \sqrt{\frac{1}{3}}P_{33}e^{i(\delta_{33}^P + \phi_3^P)},\end{aligned}\tag{7}$$

- ¹³ for $\Lambda \rightarrow n\pi^0$,

$$\begin{aligned}S(\Lambda_0) &= \sqrt{\frac{1}{3}}S_{11}e^{i(\delta_{11}^S + \phi_1^S)} + \sqrt{\frac{2}{3}}S_{33}e^{i(\delta_{33}^S + \phi_3^S)}, \\ P(\Lambda_0) &= \sqrt{\frac{1}{3}}P_{11}e^{i(\delta_{11}^P + \phi_1^P)} + \sqrt{\frac{2}{3}}P_{33}e^{i(\delta_{33}^P + \phi_3^P)},\end{aligned}\tag{8}$$

- ¹⁴ where S and P is isospin amplitudes with subscript convention $S_{2\Delta I, 2I}$ and $P_{2\Delta I, 2I}$. The average of α^Λ
¹⁵ for two modes is the same as the values in the $|\Delta I| = 1/2$ limit,

$$\alpha^\Lambda := \frac{2\alpha_\perp^\Lambda + \alpha_0^\Lambda}{3} = 2S_{11}P_{11} \cos(\phi_1^P - \phi_1^S).\tag{9}$$

Figure 1: Using `feynmp`

¹ The first order correction of $|\Delta I| = 3/2$ is given as:

$$\begin{aligned} \frac{\alpha_{-}^{\Lambda} - \alpha_0^{\Lambda}}{\alpha^{\Lambda}} &= \frac{3}{\sqrt{2}} \frac{\Delta\alpha_{3/2}}{\cos(\phi_1^P - \phi_1^S)} + 3(2s^2 - 1)\Delta_{\Lambda}, \\ \Delta\alpha_{3/2} &= p_3 \left[(1 - s^2) \cos(2\phi_1^P - \phi_1^S - \phi_3^P) - s^2 \cos(\phi_1^S - \phi_3^P) \right] \\ &\quad + s_3 \left[s^2 \cos(2\phi_1^S - \phi_1^P - \phi_3^S) - (1 - s^2) \cos(\phi_1^P - \phi_3^S) \right] \end{aligned} \quad (10)$$

² where $s := S_{11}$, $s_3 := S_{33}/S_{11}$, and $p_3 := P_{33}/P_{11}$. We can construct isospin averages of the observables
³ from two isospin modes to recover the results in the $|\Delta I| = 1/2$ limit and require a better precision,

$$A_{CP}^{\Lambda} := \frac{2A_{CP}^{-} + A_{CP}^{0}}{3} = -\tan(\delta_{11}^P - \delta_{11}^S) \tan(\phi_1^P - \phi_1^S). \quad (11)$$

⁴ The CP observables A_{CP}^{Ξ} and ϕ_{CP}^{Ξ} of Ξ^- can also be measured to have a cross check with the charged
⁵ channel measurement.

6 1.1 Previous results

⁷ The decay process $J/\psi \rightarrow \Xi^- \bar{\Xi}^+$ belongs to family $J/\psi \rightarrow Y\bar{Y}$, where Y stands for hyperon Λ , Σ , and
⁸ Ξ . These decay processes are published or ongoing at BESIII collaboration. The results of the charged
⁹ channel of $J/\psi \rightarrow \Xi^- \bar{\Xi}^+$ and $J/\psi \rightarrow \Lambda \bar{\Lambda}$ are list in Table 1.

Table 1: **Summary of results.**

Parameter	BESIII result	Previous result
α_ψ	$0.586 \pm 0.012 \pm 0.010$	$0.58 \pm 0.04 \pm 0.08$ [?]
$\Delta\Phi$	$1.213 \pm 0.046 \pm 0.016$ rad	–
α_Ξ	$-0.376 \pm 0.007 \pm 0.003$	-0.401 ± 0.010 [?]
ϕ_Ξ	$0.011 \pm 0.019 \pm 0.009$ rad	-0.037 ± 0.014 rad [?]
$\bar{\alpha}_\Xi$	$0.371 \pm 0.007 \pm 0.002$	–
$\bar{\phi}_\Xi$	$-0.021 \pm 0.019 \pm 0.007$ rad	–
α_-^Λ	$0.757 \pm 0.011 \pm 0.008$	$0.750 \pm 0.009 \pm 0.004$ [?]
$\bar{\alpha}_+^\Lambda$	$-0.763 \pm 0.011 \pm 0.007$	$-0.758 \pm 0.010 \pm 0.007$ [?]
α_0^Λ	–	0.74 ± 0.05
$\bar{\alpha}_0^\Lambda$	$-0.692 \pm 0.016 \pm 0.006$	–
$\xi_P - \xi_S$	$(1.2 \pm 3.4 \pm 0.8) \times 10^{-2}$ rad	–
$\delta_P - \delta_S$	$(-4.0 \pm 3.3 \pm 1.7) \times 10^{-2}$ rad	$(10.2 \pm 3.9) \times 10^{-2}$ rad [?]
A_{CP}^Ξ	$(6.0 \pm 13.4 \pm 5.6) \times 10^{-3}$	–
$\Delta\phi_{\text{CP}}^\Xi$	$(-4.8 \pm 13.7 \pm 2.9) \times 10^{-3}$ rad	–
A_{CP}^Λ	$(-3.7 \pm 11.7 \pm 9.0) \times 10^{-3}$	$(-6 \pm 12 \pm 7) \times 10^{-3}$ [?]
$\langle \phi_\Xi \rangle$	$0.016 \pm 0.014 \pm 0.007$ rad	

2 Data Sample

2.1 BESIII Detector

The BESIII detector [2] records symmetric e^+e^- collisions provided by the BEPCII storage ring [3], which operates with a peak luminosity of $1 \times 10^{33} \text{ cm}^{-2}\text{s}^{-1}$ in the center-of-mass energy range from 2.0 to 4.95 GeV. BESIII has collected large data samples in this energy region [4]. The cylindrical core of the BESIII detector covers 93% of the full solid angle and consists of a helium-based multilayer drift chamber (MDC), a plastic scintillator time-of-flight system (TOF), and a CsI(Tl) electromagnetic calorimeter (EMC), which are all enclosed in a superconducting solenoidal magnet providing a 1.0 T (0.9 T in 2012) magnetic field. The solenoid is supported by an octagonal flux-return yoke with resistive plate counter muon identification modules interleaved with steel. The charged-particle momentum resolution at $1 \text{ GeV}/c$ is 0.5%, and the dE/dx resolution is 6% for electrons from Bhabha scattering. The EMC measures photon energies with a resolution of 2.5% (5%) at 1 GeV in the barrel (end cap) region. The time resolution in the TOF barrel region is 68 ps, while that in the end cap region is 110 ps. The end cap TOF system was upgraded in 2015 using multigap resistive plate chamber technology, providing a time resolution of 60 ps [5].

2.2 Data sample

From 2009 to 2019, over 10^{10} J/ψ events were collected with BESIII detector. In 10 years, the data sets were taken at four separate time regions, donated 2009, 2012, 2018 and 2019. The number of J/ψ events is determined by using inclusive decay of the J/ψ . Table 2 shows the number of J/ψ events in each data sets. Due to the variation of detector status and reconstruction efficiency, we will perform the analysis for each data sets separately.

Table 2: The number of events for J/ψ data sets.

Data sets	Number of events
2009	$(224.0 \pm 1.3) \times 10^6$
2012	$(1088.5 \pm 4.4) \times 10^6$
2018	$(8774.0 \pm 39.4) \times 10^6$
2019	$(1088.5 \pm 4.4) \times 10^6$
Total	$(1088.5 \pm 4.4) \times 10^6$

1 2.3 Monte Carlo Simulation

2 2.3.1 Inclusive Monte Carlo

3 Simulated data samples produced with a GEANT4-based [6] Monte Carlo (MC) package, which includes
 4 the geometric description of the BESIII detector and the detector response, are used to determine detec-
 5 tion efficiencies and to estimate backgrounds. The simulation models the beam energy spread and initial
 6 state radiation (ISR) in the e^+e^- annihilations with the generator KKMC [7].

- 7 • the J/ψ data set

8 The inclusive MC sample includes both the production of the J/ψ resonance and the continuum
 9 processes incorporated in KKMC [7].

10 All particle decays are modelled with EVTGEN [8] using branching fractions either taken from the Particle
 11 Data Group [9], when available, or otherwise estimated with LUNDCHARM [10]. Final state radiation (FSR)
 12 from charged final state particles is incorporated using the PHOTOS package [11].

13 2.3.2 Signal Monte Carlo

14 The following Monte Carlo samples are also been generated by ourselves.

15 Phase space (PHSP MC) for two decay channel were generated for calculating the normalization in
 16 the maximum log likelihood method.

17 Signal MC samples simulated using the parameters estimated from data (mDIY MC) were generated
 18 as a control sample searching for inconsistencies between data and MC and used for input/output check
 19 and selection criteria optimization. These values are within the fit uncertainties of the experimentally
 20 obtained values and CP-conservation is assumed. The true distributions of the momentum of final states
 21 and 16 production moments are plotted in Fig. 26, 27, 32, 33. (For the four sets of MC simulation, the
 22 distributions are very similar. We only use 2009 MC sets as an example to show the distributions. The
 23 distributions of others can be found in Appendix. A.)

24 The number of events of PHSP MC and mDIY MC samples are decided according to the number
 25 of J/ψ events and the branching fraction $\mathcal{B}(J/\psi \rightarrow \Xi^-\bar{\Xi}^+) = (9.7 \pm 0.8) \times 10^{-4}$, $\mathcal{B}(\Xi^- \rightarrow \Lambda\pi^-) =$
 26 $(99.887 \pm 0.035)\%$, $\mathcal{B}(\Lambda \rightarrow p\pi^-) = (63.9 \pm 0.5)\%$, and $\mathcal{B}(\Lambda \rightarrow n\pi^0) = (35.8 \pm 0.5)\%$. There is no doubt
 27 that the more statistic the MC has, the better for analysis. Taking CPU time into account, we decide to
 28 generate a PHSP MC sample and a mDIY MC sample with 30 times the corresponding experimental
 29 data statistic. The number of event of MC samples for different years are listed in Table. 3.

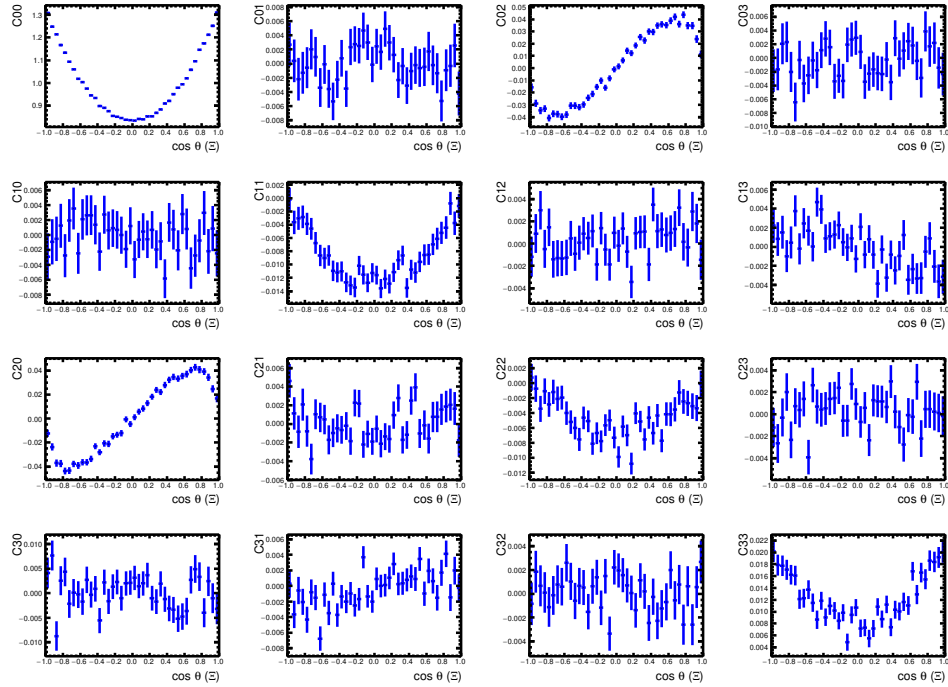


Figure 2: Using 2009 mDIY MC as example to show the true distributions of the 16 moments of neutron channel for $J/\psi \rightarrow \Xi^- \bar{\Xi}^+$.

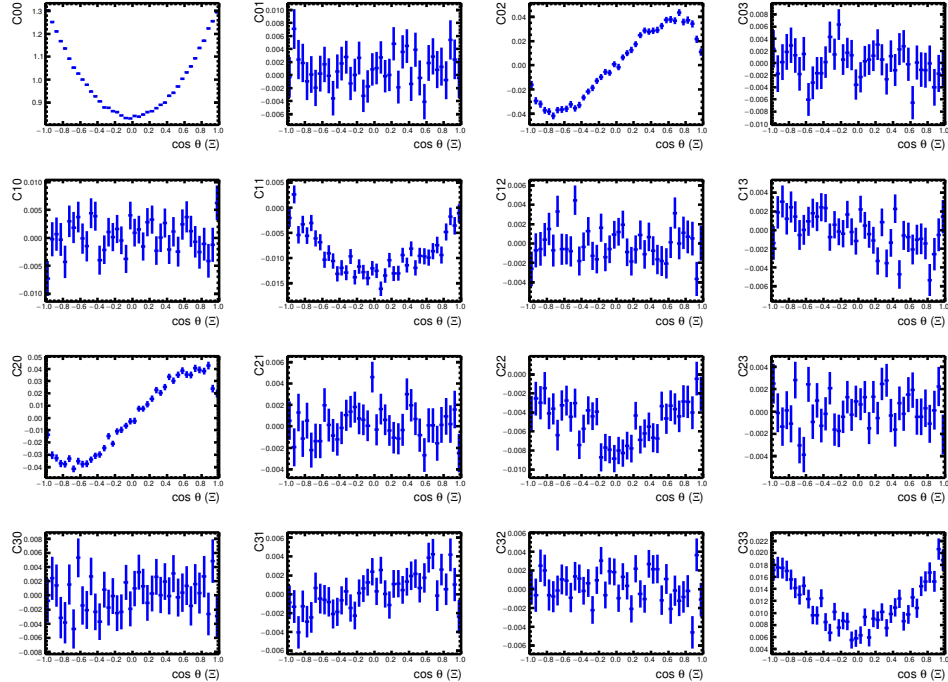


Figure 3: Using 2009 mDIY MC as example to show the true distributions of the 16 moments of anti-neutron channel for $J/\psi \rightarrow \Xi^- \bar{\Xi}^+$.

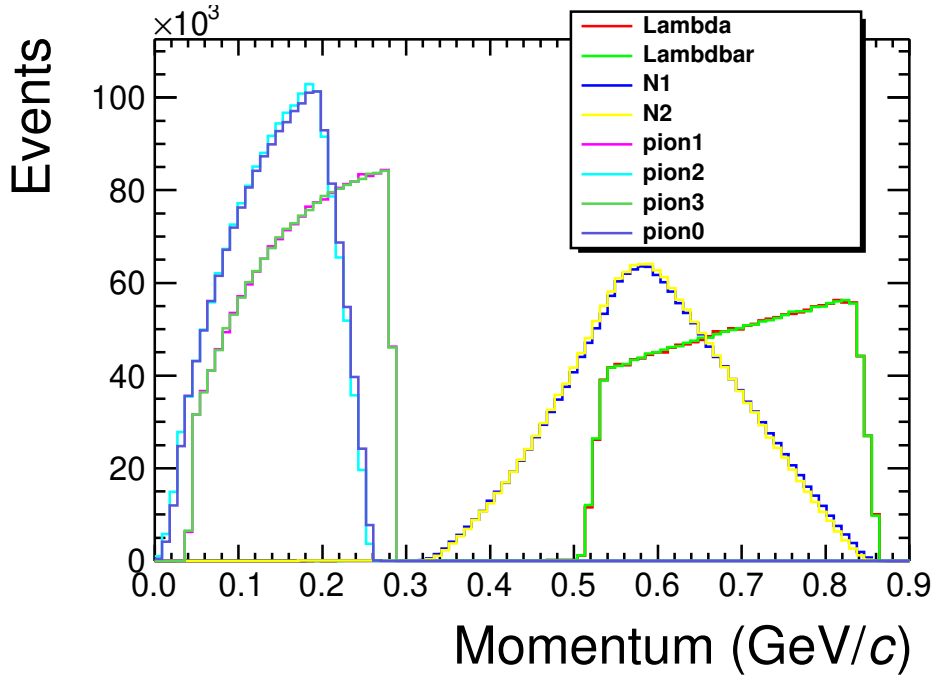


Figure 4: Using 2009 mDIY MC as example to show the true momentum of final states and Λ resonances in neutron channel for $J/\psi \rightarrow \Xi^- \bar{\Xi}^+$. The order of final states in legend is Λ , $\bar{\Lambda}$, n , \bar{p} , π_Ξ^+ , π_Λ^+ , π_Ξ^- , and π^0 .

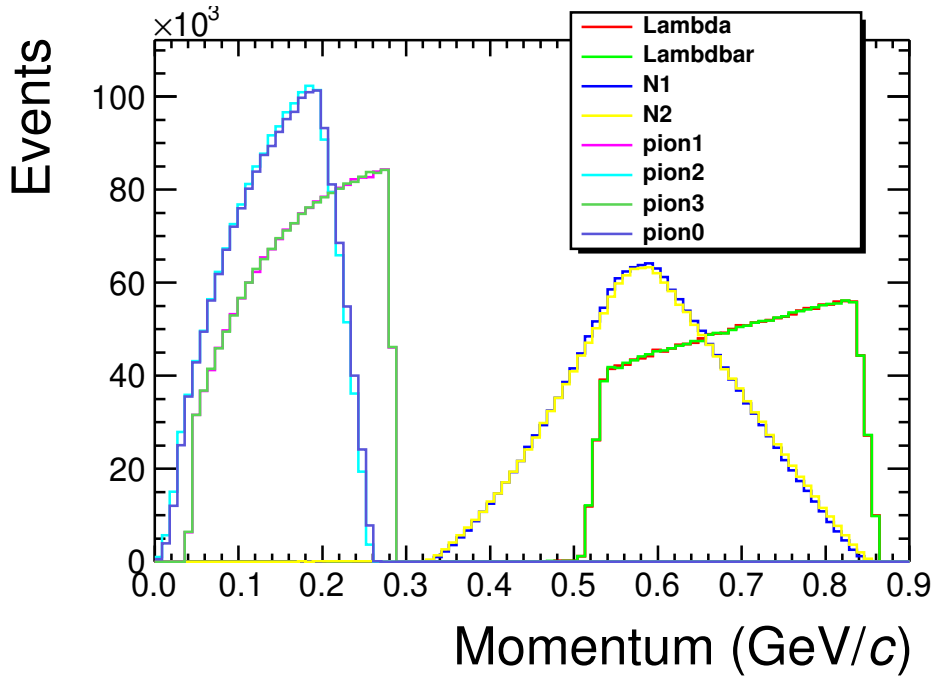


Figure 5: Using 2009 mDIY MC as example to show the true momentum of final states and Λ resonances in anti-neutron channel for $J/\psi \rightarrow \Xi^- \bar{\Xi}^+$. The order of final states in legend is Λ , $\bar{\Lambda}$, p , \bar{n} , π_Ξ^- , π_Λ^- , π_Ξ^+ , and π^0 .

Table 3: The number of events for PHSP MC and mDIY MC samples.

Data sets	PHSP MC (million)	mDIY MC (million)
2009	1.8	1.8
2012	9	9
2018	37.8	37.8
2019	37.8	37.8
Total	86.4	86.4

3 Event Selection

3.1 Quick review

3.2 Track level selection

- **Good charged track**

- Charged tracks detected in the MDC are required to be within a polar angle (θ) range of $|\cos\theta| < 0.93$, where θ is defined with respect to the z -axis, which is the symmetry axis of the MDC.
- Due to the long life time of Ξ and Λ , for charged tracks in final states, the distance of closest approach to the interaction point (IP) must be less than 30 cm along the z -axis, $|V_z|$, and less than 10 cm in the transverse plane, $|V_{xy}|$.
- The total number of charged tracks should be equal to 4. This requirement can help us reducing the background caused by charged channel $J/\psi \rightarrow \Xi^-\bar{\Xi}^+ \rightarrow \Lambda(\rightarrow p\pi^-)\pi^-\bar{\Lambda}(\rightarrow \bar{p}\pi^+)\pi^+$.

- **Good photon selection**

- Photon candidates are identified using showers in the EMC. The deposited energy of each shower must be more than 25 MeV in the barrel region ($|\cos\theta| < 0.80$) and more than 50 MeV in the end cap region ($0.86 < |\cos\theta| < 0.92$).
- To exclude showers that originate from charged tracks, the angle subtended by the EMC shower and the position of the closest charged track at the EMC must be greater than 20 degrees as measured from the IP.
- To suppress electronic noise and showers unrelated to the event, the difference between the EMC time and the event start time is required to be within [0, 700] ns.
- There is an additional requirement for neutron channel. To veto the shower deposited by neutrons in the EMC, the opening angle between the direction of Λ and the direction of a photon shower must be greater than 15 degrees. However, anti-neutron channel doesn't need such requirement. It will be discussed in the following sub-section.

- **Particle identification**

- One proton/anti-proton, two π^-/π^+ , and one π^+/π^- must be identified for neutron/anti-neutron channel. According to the true information as shown in Fig. 32, 33, the proton and pion

1 candidates must have momenta $p_{pr} > 0.32 \text{ GeV}/c$ and $p_\pi < 0.30 \text{ GeV}/c$, respectively. There
 2 is no overlap between proton and pion momenta. The comparison of reconstruction momenta
 3 between data and MC are shown in Fig. ?? ???. The alternative would be to use particle
 4 identification methods. As discussed in [], this method is not considered viable.

5 3.3 Event level selection

6 For both neutron channel and anti-neutron channel, there is two legs, a charged leg $\Xi^- \rightarrow \Lambda(\rightarrow p\pi^-)\pi^-$
 7 or c.c. and a neutral leg $\bar{\Xi}^+ \rightarrow \bar{\Lambda}(\rightarrow \bar{n}\pi^0)\pi^+$ or c.c.. A so called single tag double tag method are used to
 8 reconstruct the decay process from the available pool of charged tracks and photon showers. Single tag
 9 is used to reconstruct the charged leg and double tag is used to reconstruct the neutral lag.

10 • Single tag

- 11 – The Λ candidate is reconstructed from proton and charged pion and required to pass a primary
 12 vertex fit.
- 13 – The Ξ candidate reconstructed from the Λ and the remaining pion is required to pass a pri-
 14 mary and a secondary vertex fit. The secondary vertex fit for the Λ is set at the decay point
 15 of Ξ , for the formed Ξ is set at the interaction point.
- 16 – The charged combination is selected to minimize $\Delta m_{\Xi\Lambda} = ((m_{p\pi\pi} - m_\Xi)^2 + (m_{p\pi} - m_\Lambda)^2)^{1/2}$,
 17 where $m_{p\pi\pi}$ and $m_{p\pi}$ denote the reconstructed invariant masses of the proton-pion-pion and
 18 proton-pion systems, respectively and m_Ξ , m_Λ are the PDG tabulated masses of Ξ and Λ ,
 19 respectively.

20 • Double tag

- 21 – The π^0 candidate is reconstructed from a pair of photons which survive the good photon
 22 selections. An unconstrained mass $M(\gamma\gamma)$ is calculated from energies and momenta of two
 23 photon pairs and it must be within $M(\pi^0) - 0.06 < M(\gamma\gamma) < M(\pi^0) + 0.04$. A kinematic
 24 fit of the two photons is also performed with a constraint $M(\gamma\gamma) = M(\pi^0)$. The chi^2 from
 25 kinematic fit must be less than 25. And the resulting energies and momenta of π^0 is saved for
 26 further analyses.
- 27 – A kinematic fit with the following constraints is performed to suppress background and im-

1 prove the resolution especially for final states in neutral leg,

$$P_{J/\psi} = P_{\Xi^\pm} + P_{\pi^\mp + P_{\gamma_1}} + P_{\gamma_2} + P_{n/\bar{n}}, \quad (12a)$$

$$M(\pi^0) = M(\gamma_1 \gamma_2), \quad (12b)$$

$$M(\Lambda/\bar{\Lambda}) = M(\gamma_1 \gamma_2 n/\bar{n}), \quad (12c)$$

2 where P stands for the four-momenta, M stands for the invariant mass, γ_1 and γ_2 is the photon
 3 from π^0 in energy descending order. The χ^2 from the kinematic fit is required to be less than
 4 200.

5 • **An additional requirement for neutron channel**

- 6 – As mentioned before, the shape of neutron shower is very similar with one of a photon
 7 shower. The neutron shower has a possibility to pass the good photon selections and form
 8 a π^0 candidate with a small energy photon. As shown in Fig. 6, the true opening angle
 9 between Λ and n (or, $\bar{\Lambda}$ and \bar{n}) is less than 0.25 rad. Figure 7 show the open angle between
 10 Λ and photons after reconstruction. For the neutron channel, the peaks at 0.15 rad is caused
 11 by neutron shower being mistaken for photon shower. There is no such problem for anti-
 12 neutron channel. In order to void the mistaken of neutron showers, an angle cut for Λ and
 13 the EMC showers is required. When we select photons from the EMC shower queues, with
 14 four momenta of Λ which is obtained by the energy-momentum conservation in the recoiling
 15 system of $\bar{\Xi}$ and π^- , the open angle between Λ and the EMC showers can be calculated and
 16 will be required to be less than 15° .

17 **3.4 Further selection**

18 After the initial selection criteria one is left with a sample that needs to be polished further. In order
 19 to reduce background contributions and reduce data-Monte Carlo discrepancies, the following selection
 20 criteria have been applied.

21 • **Further selection criteria**

- 22 – requiring that the reconstructed decay lengths of all final state hyperons are greater than 0;
- 23 – requiring that the cosine of the angle of the reconstructed Ξ^- in the center-of-mass frame,
 24 $\cos \theta_{\Xi^-, \text{CM}}$, fulfills the requirement $|\cos \theta_{\Xi^-, \text{CM}}| < 0.84$.

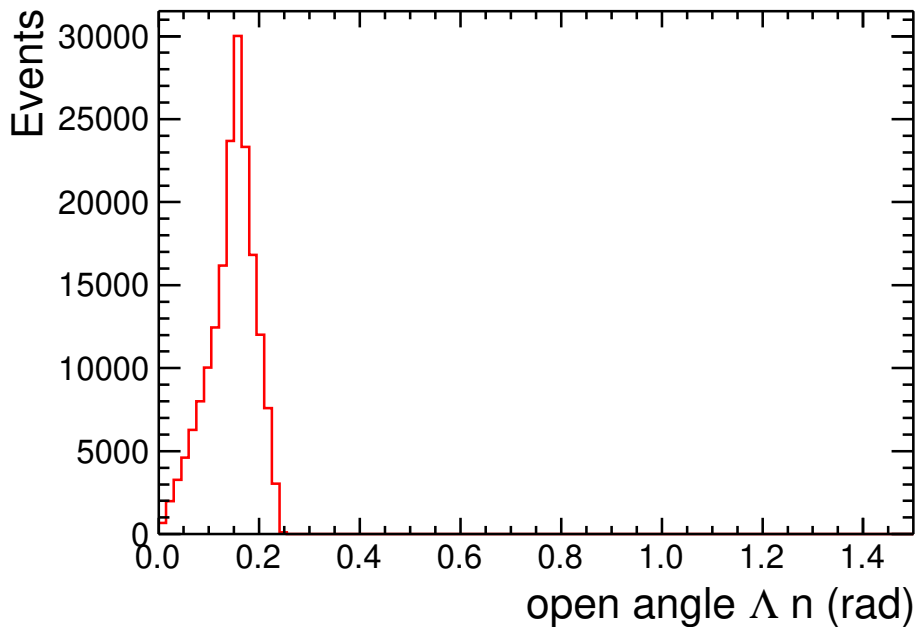


Figure 6

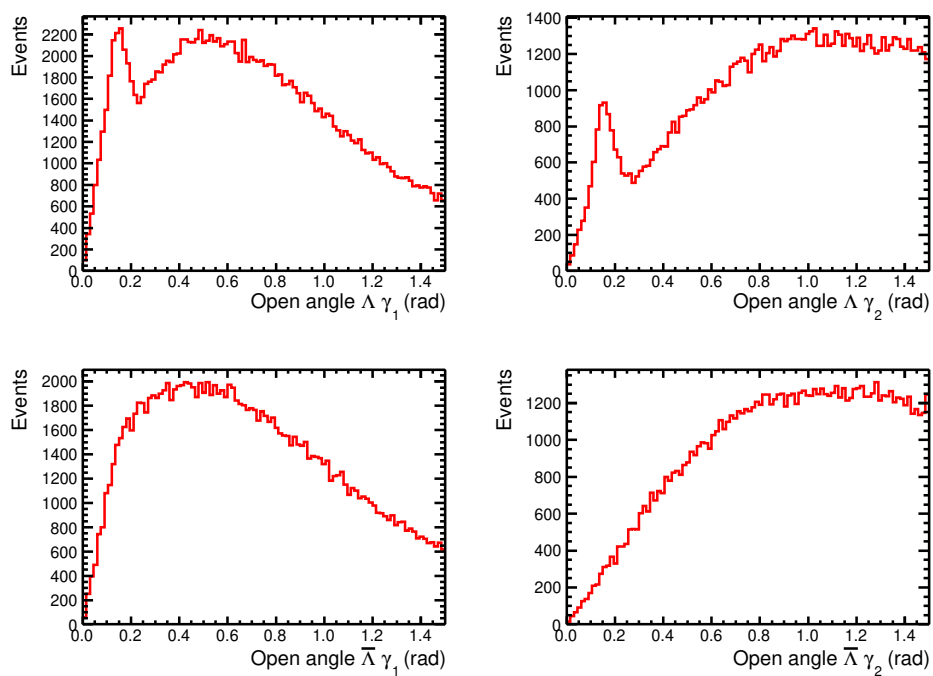


Figure 7

- 1 – setting a mass window selection criteria for the Λ candidates. For the neutron channel, we re-
- 2 quire that $|M(\bar{p}\pi^+)| < 0.0115 \text{ GeV}/c^2$, for the anti-neutron channel, $|M(p\pi^-)| < 0.0115 \text{ GeV}/c^2$.
- 3 – setting a mass window selection criteria for the Ξ^- and $\bar{\Xi}^+$ candidates. For the neutron
- 4 channel, we require that $|M(n\gamma\gamma\pi^-)| < 0.011 \text{ GeV}/c^2$, $|M(\bar{p}\pi^+\pi^+)| < 0.011 \text{ GeV}/c^2$; for the
- 5 anti-neutron channel, $|M(\bar{n}\gamma\gamma\pi^+)| < 0.011 \text{ GeV}/c^2$, $|M(p\pi^-\pi^-)| < 0.011 \text{ GeV}/c^2$.

4 Background estimation

4.1 Inclusive MC

The potential backgrounds from other decay processes that might be present in the data are studied by analyzing the official inclusive MC sample. After final events selection, a topology method is used to classify the survived events. Table 4 lists the dominantly contributing processes for two decay channels and four data sets. Three variables $M(\Xi^-)$, $M(\bar{\Xi}^+)$ and $M(n/\bar{n})$ are used to separate the signal and background. If a background channel has very similar shapes in these three mass spectra with the signal shapes, it is called a peaking background. They can be categorized into three groups: charged decay channel, peaking background, and non-peaking background.

Table 4

No.	Decay tree	2009	2012	2018	2019
1	$J/\psi \rightarrow \eta_c \gamma, \eta_c \rightarrow \bar{\Xi}^+ \Xi^-, \bar{\Xi}^+ \rightarrow \pi^+ \bar{\Lambda}, \Xi^- \rightarrow \pi^- \Lambda, \bar{\Lambda} \rightarrow \pi^+ \bar{p}$,	28	178	611	535
2	$J/\psi \rightarrow \pi^+ \pi^- \Lambda \bar{\Lambda}, \Lambda \rightarrow \pi^0 n, \bar{\Lambda} \rightarrow \pi^+ \bar{p}$	23	108	429	348
3	$J/\psi \rightarrow \bar{\Xi}^+ \Xi^-, \bar{\Xi}^+ \rightarrow \pi^+ \bar{\Lambda}, \Xi^- \rightarrow \pi^- \Lambda, \bar{\Lambda} \rightarrow \pi^+ \bar{p}, \Lambda \rightarrow \pi^- p$	4	21	86	113
4	Others	20	197	434	340

Table 5

No.	Decay tree	2009	2012	2018	2019
1	$J/\psi \rightarrow \eta_c \gamma, \eta_c \rightarrow \bar{\Xi}^+ \Xi^-, \bar{\Xi}^+ \rightarrow \pi^+ \bar{\Lambda}, \Xi^- \rightarrow \pi^- \Lambda, \bar{\Lambda} \rightarrow \pi^0 \bar{n}$,	30	175	612	345
2	$J/\psi \rightarrow \pi^+ \pi^- \Lambda \bar{\Lambda}, \Lambda \rightarrow \pi^- p, \bar{\Lambda} \rightarrow \pi^0 \bar{n}$	17	114	373	253
3	$J/\psi \rightarrow \bar{\Xi}^+ \Xi^-, \bar{\Xi}^+ \rightarrow \pi^+ \bar{\Lambda}, \Xi^- \rightarrow \pi^- \Lambda, \bar{\Lambda} \rightarrow \pi^+ \bar{p}, \Lambda \rightarrow \pi^- p$	6	20	200	149
4	Others	18	123	431	235

The charged decay channel has been well studied. The mDIY MC samples for charged decay channel are generated according to [1]. The mass spectra of $M(\Xi^-)$, $M(\bar{\Xi}^+)$ and $M(n/\bar{n})$ for this channel are plotted in Fig. 8. Figure 9 shows the 2D mass distribution $M(\Xi^-)$ v.s. $M(\bar{\Xi}^+)$. This background will be subtracted in the maximum log likelihood fit.

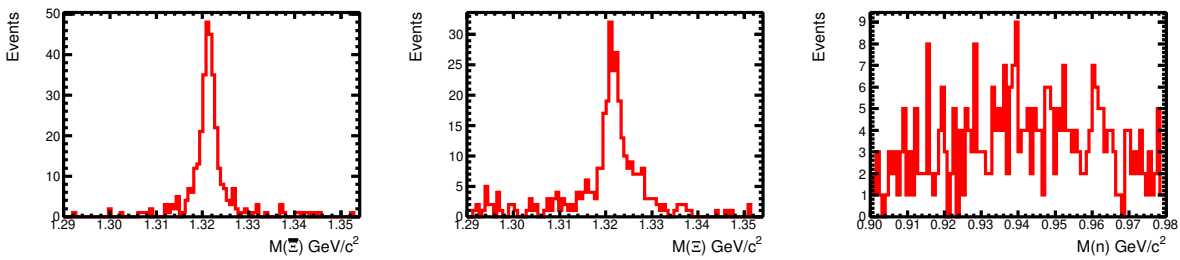


Figure 8

1 The exclusive decay $J/\psi \rightarrow \eta_c \gamma \rightarrow \Xi^-\bar{\Xi}^+\gamma$ is a peaking background. According to PDG, the related
 2 branch fractions are $\mathcal{B}(J/\psi \rightarrow \eta_c \gamma) = (17 \pm 0.4)\%$ and $\mathcal{B}(\eta_c \rightarrow \Xi^-\bar{\Xi}^+) = (9.0 \pm 2.6) \times 10^4$. The process
 3 $e^-e^+ \rightarrow J/\psi \rightarrow \eta_c \gamma$ has a angular distribution $1 + \cos^2 \theta$. The spin density matrix for $\eta_c \rightarrow \Xi^-\bar{\Xi}^+$ is
 4 $\text{diag}(1, -1, 1, 1)$. The decay matrix for the hyperons have been discussed in Sec. ???. A mDIY MC sample
 5 with 30 number of events are generated to estimate the background in the data.

6 For the phase space decay $J/\psi \rightarrow \pi^+\pi^-\Lambda\bar{\Lambda}$ and the rest decay channels, figure 10 11 show the distri-
 7 butions of variables $M(\Xi^-)$, $M(\bar{\Xi}^+)$ and $M(n/\bar{n})$. Since the shapes for $M(\Xi^-)$ and $M(\bar{\Xi}^+)$ are continuous
 8 and flat, a sideband method will be used to estimate this background.

9 **4.2 Miscombination background**

10 When the π^0 are reconstructed from the EMC photon shower queues, there is a probability that one or
 11 both of the photon showers are noise or fake photons. That event might survive the final event selection.
 12 Although it is a real signal event, the miscombination of photon will lead to a false four momenta of π^0
 13 and a wrong angular reconstruction of neutron or anti-neutron. A photon matched angle is used to judge
 14 if the reconstructed photon is correct or not, which is defined as following: there are two photons in the
 15 MC truth, γ_{true}^1 and γ_{true}^2 , and two reconstructed photons γ_{rec}^1 and γ_{rec}^2 . If $\theta(\gamma_{\text{true}}^1, \gamma_{\text{rec}}^1) + \theta(\gamma_{\text{true}}^2, \gamma_{\text{rec}}^2) <$
 16 $\theta(\gamma_{\text{true}}^1, \gamma_{\text{rec}}^2) + \theta(\gamma_{\text{true}}^2, \gamma_{\text{rec}}^1)$, then, the matched angle for photon 1 and photon 2 is $\theta_{\text{match}}^1 = \theta(\gamma_{\text{true}}^1, \gamma_{\text{rec}}^1)$
 17 and $\theta_{\text{match}}^2 = \theta(\gamma_{\text{true}}^2, \gamma_{\text{rec}}^2)$, respectively; else $\theta_{\text{match}}^1 = \theta(\gamma_{\text{true}}^1, \gamma_{\text{rec}}^2)$, $\theta_{\text{match}}^2 = \theta(\gamma_{\text{true}}^2, \gamma_{\text{rec}}^1)$. Figure 12 show
 18 the distributions of the photon matched angle. It's obvious that the matched angle for some photons are
 19 too large to be correct. At the stage of MC study, requirements on photon matched angle $\theta_{\text{match}}^1 < 0.3$ rad
 20 and $\theta_{\text{match}}^2 < 0.3$ rad can be applied to separate the signal and mis-combination background. As shown
 21 in Fig. 13, the shape of mis-combination background are relatively flat compared to one of the signal.
 22 It can be used as a variable to distinguish between signal and background. It is also expectable that the
 23 shapes of signal and background are very similar for $M(\Xi^-)$, $M(\bar{\Xi}^+)$ and $M(\Lambda)$.

24 Figure 14 show that the mis-combination background will lead to a worse resolution of the recon-
 25 struction of neutron/anti-neutron position. A large mDIY MC sample will be used to estimate the mis-
 26 combination background.

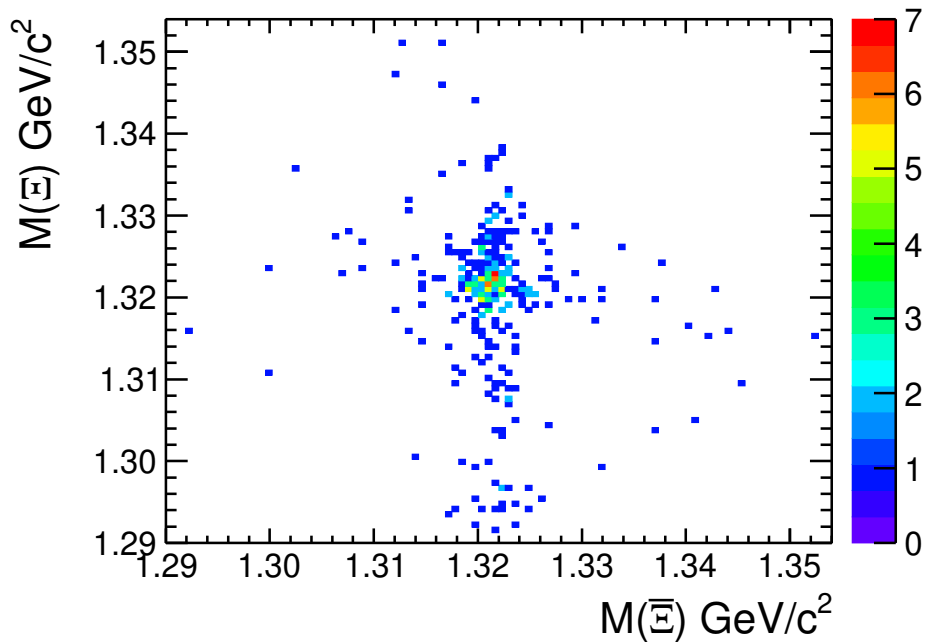


Figure 9

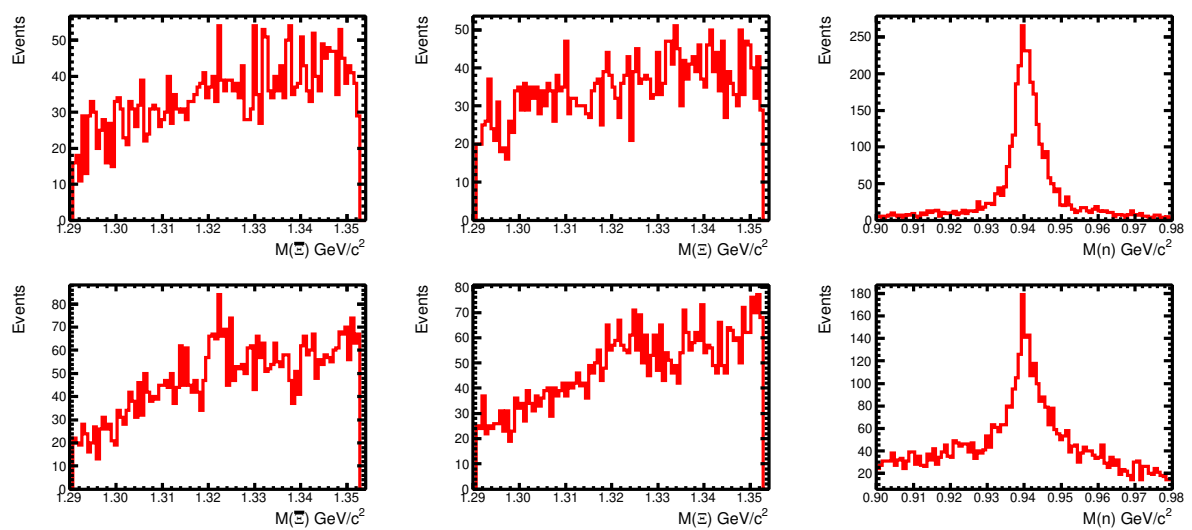


Figure 10

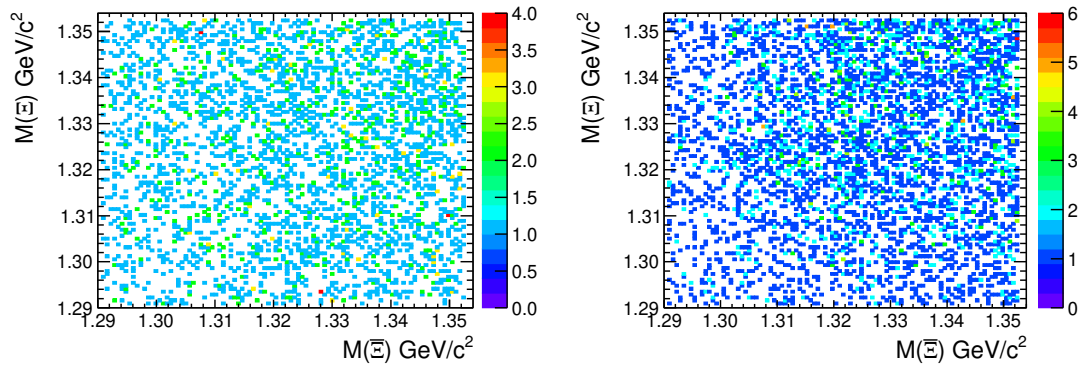


Figure 11

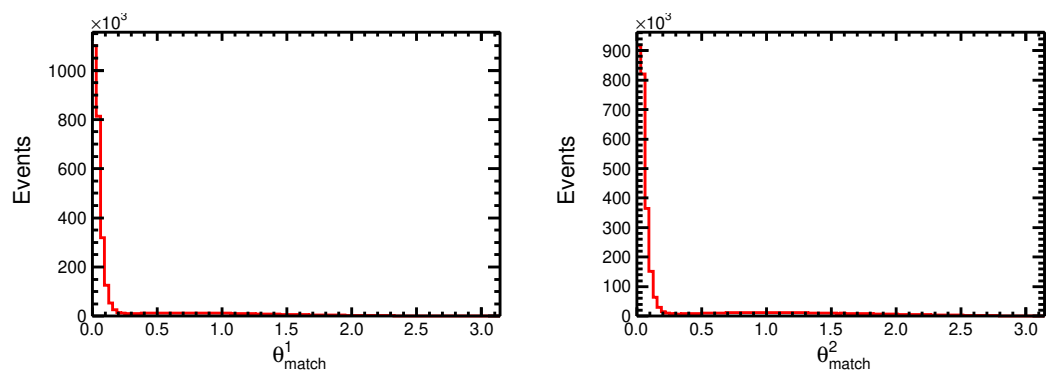


Figure 12

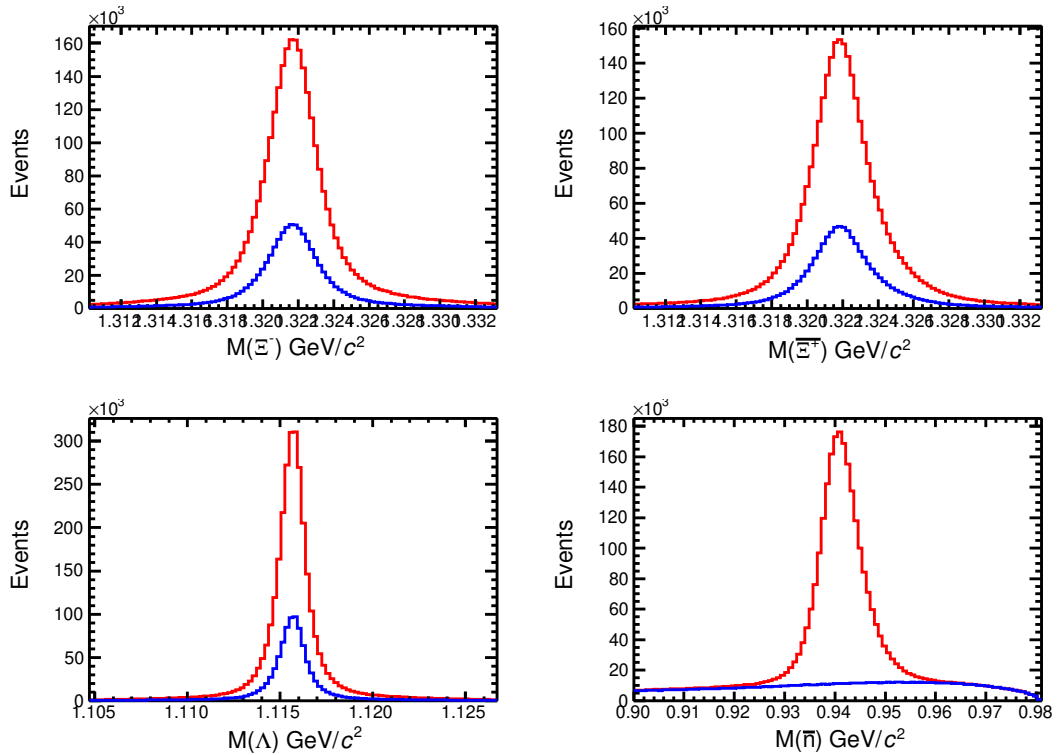


Figure 13

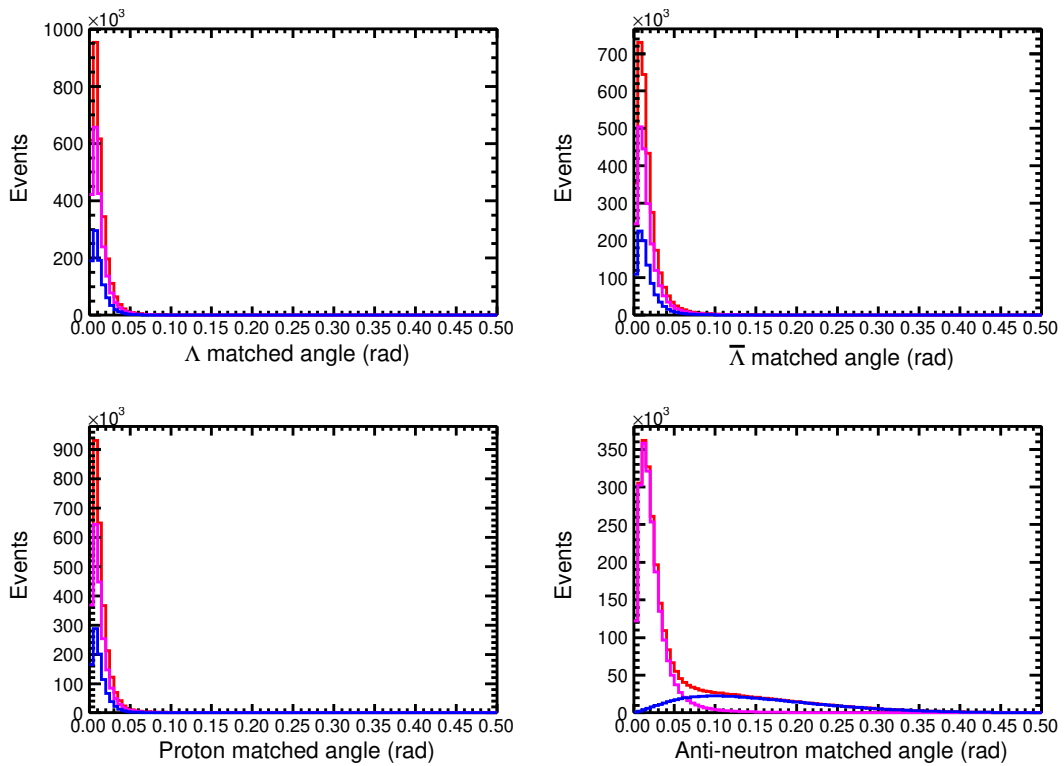


Figure 14

1 5 Parameters estimation

2 5.1 Maximum likelihood fit

3 A maximum likelihood fit is used to extract the decay parameters, which are only related to the helicity
 4 angles. For each channel, the probability distribution function (PDF) with eight unknown parameters Ω
 5 can be defined in nine dimensions helicity angles spanned by ξ :

$$\mathcal{P}(\xi; \Omega) = \mathcal{W}(\xi; \Omega)\varepsilon(\xi)/\mathcal{N}(\Omega) \quad (13)$$

6 The full likelihood function can be written as

$$\mathcal{S} = - \sum_{i=1}^N \ln \mathcal{W}(\xi_i; \Omega) + \sum_j \sum_i^{N_j^{\text{bkg}}} \ln \mathcal{W}(\xi_i; \Omega) + N^{\text{signal}} \times \ln \mathcal{N}(\Omega) - \sum_i^N \ln \varepsilon(\xi_i) \quad (14)$$

- 7 • Helicity angles and parameters

8 For neutron channel, the helicity angles $\xi = (\theta_\Xi, \theta_\Lambda, \phi_\Lambda, \theta_{\bar{\Lambda}}, \phi_{\bar{\Lambda}}, \theta_n, \phi_n, \theta_{\bar{p}}, \phi_{\bar{p}})$ and the parameters
 9 $\Omega = (\alpha_{J/\psi}, \Delta\Phi, \alpha_{\Xi^-}, \phi_{\Xi^-}, \alpha_{\Xi^+}, \phi_{\Xi^+}, \alpha_\Lambda^0, \alpha_{\bar{\Lambda}}^+);$

10 For anti-neutron channel, the helicity angles $\xi = (\theta_\Xi, \theta_\Lambda, \phi_\Lambda, \theta_{\bar{\Lambda}}, \phi_{\bar{\Lambda}}, \theta_p, \phi_p, \theta_{\bar{n}}, \phi_{\bar{n}})$ and the parameters
 11 $\Omega = (\alpha_{J/\psi}, \Delta\Phi, \alpha_{\Xi^-}, \phi_{\Xi^-}, \alpha_{\Xi^+}, \phi_{\Xi^+}, \alpha_\Lambda^-, \alpha_{\bar{\Lambda}}^0).$

- 12 • $-\sum_{i=1}^N \ln \mathcal{W}(\xi_i; \Omega)$

13 The first item is the sum of all events (total N events) which survive the final selection criteria in
 14 experiment data. $\mathcal{W}(\xi_i; \Omega)$ is the amplitude value for i -th events. In practice, we will try to find
 15 minimum value of a function. So, there is a negative sign in the PDF.

- 16 • $\sum_j \sum_i^{N_j^{\text{bkg}}} \ln \mathcal{W}(\xi_i; \Omega)$

17 The second item stands for the background subtracting. There are total $j = 4$ types of background:
 18 mis-combination background, charged decay channel, $J/\psi \rightarrow \gamma\eta_c$ and non-peaking background.

19 N_j^{bkg} is the estimated number of events for j -th type of background.

- 20 • $N^{\text{signal}} \times \ln \mathcal{N}(\Omega)$

21 $\mathcal{N}(\Omega)$ is the normalization factor given by:

$$\mathcal{N}(\Omega) = \int \mathcal{W}(\xi; \Omega)\varepsilon(\xi)d\xi \quad (15)$$

22 In practice, there are two methods to calculate the normalization factor, using PHSP MC or mDIY
 23 MC, propagated through the detector and reconstructed as data. The normalization factor calcu-

lated with PHSP MC is approximately given as:

$$\mathcal{N}(\Omega) = \frac{1}{M} \sum_{j=1}^M \mathcal{W}(\xi_j; \Omega) \quad (16)$$

By using mDIY MC, the normalization factor is given as:

$$\mathcal{N}(\Omega) = \frac{1}{M} \sum_{j=1}^M \frac{\mathcal{W}(\xi_j; \Omega)}{\mathcal{W}(\xi_j; \Omega_0)} \quad (17)$$

where M is the total number of events of the corresponding MC sample that survived all the event selection criteria as data and with additional photon matched angle requirement..

Comments on normalization factor

- $-\sum_i^N \ln \epsilon(\xi_i)$

The last item is the efficiencies which is not dependent on the parameters in Ω and will only affects the overall log-likelihood normalization. Therefore, this item is a constant and can be dropped.

5.2 Input-Output check

An input-output check is performed to guarantee the correctness of fitting procedure. 30 sets of mDIY MC is used to do the input-output check and the number of events of each set is equal to the signal yield from data. The backgrounds are also considered by including the background events from the inclusive and exclusive MC and then using the same method as used in data to subtract the background. Table ?? lists the input-output value. The distributions of the fitting results and the pull distribution are shown in Fig. ?? . It is clear to see that the output values are consistent with the input.

1 6 Real data

2 6.1 Blind analysis

3 In order to reduce the experimenter's bias, this measurement adopts a blind analysis technique [1]. As
 4 discussed in Sec. 2.3 and Sec. 4, the signal MC and background MC are generated according to the
 5 knowledge that we have learned from previous experiments. The events selections in Sec. 3 are optimized
 6 according to the MC simulation without looking at the data. The total measurement procedure is fixed
 7 on a sub-sample of the data, 2009 + 2012 + 1/3 of 2018 and 2019 data samples. The systematic impact
 8 of the differences between MC and data are studied by applying a hidden answer method. Once all the
 9 strategies are settled, it will be performed to the full data sets to open the hidden box. The follows are
 10 the comparisons of distribution between data and MC which show the agreement of them.

11 6.2 Signal yield

12 According to the discussion in Sec. 4, the invariant mass of neutron/anti-neutron is chosen as a variable
 13 to obtain the signal yield, with an unbinned maximum likelihood fit. The signal shape is modeled as the
 14 likelihood function by a tool RooKEYSPDF in RooFit to describe the signal. As shown in Fig. 48, the shape
 15 of the miscombination background drops rapidly from 0.96 to 0.98 GeV/c². A standard argus function
 16 is not enough to describe it. We choose the product of an argus function and a 3rd order polynomial to
 17 model this background shape.

18 In the fit of the invariant mass of neutron/anti-neutron, the parameters for the background function is
 19 fixed by fitting the background shape which is from mDIY MC. The blue line in Fig. 48 is the parametric
 20 background shape. The full likelihood function is the sum of background function and signal shape
 21 convolved with a Gaussian function. The results of fit is show in Fig 48. The background have to be
 22 subtrack from this fit results. The signal yield is calculated as follow equation:

$$N_{\text{sig}} = N_{\text{fit}} - N_{\text{sideband}} - N_{\text{peaking}}, \quad (18)$$

23 where N_{sideband} is the background events estimated by a sideband method which is defined as shown
 24 in Fig. 16. N_{peaking} is the number of events of peaking background channel $J/\psi \rightarrow \gamma\eta_c$, which is esti-
 25 mated with a exclusive MC simulation.

26 6.3 Variables comparison

27 The agreement between data and MC of the variables which are used as event selection requirements to
 28 suppress the background are necessary to be checked. Figure 17 take the neutron channel in 2012 as an
 29 example to show that distributions in a order 1) $\bar{\Lambda}$ decay length, 2) $\bar{\Xi}^+$ decay length, 3) $\bar{\Xi}^+$ invariant mass,

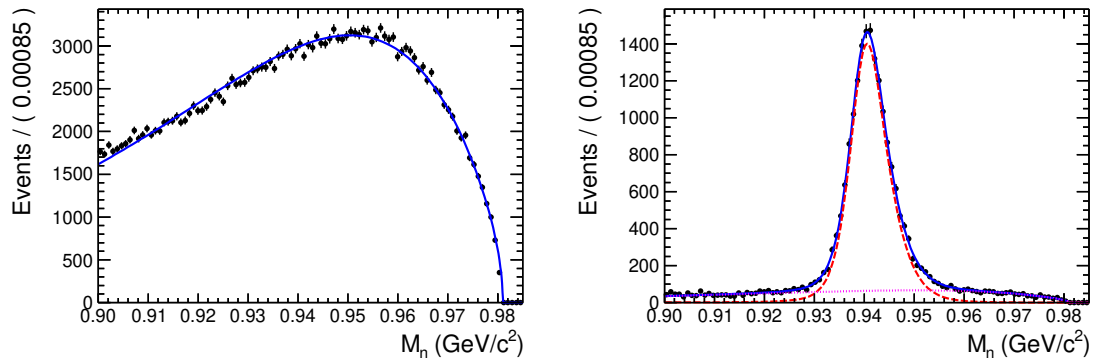


Figure 15: 2012 neutron channel

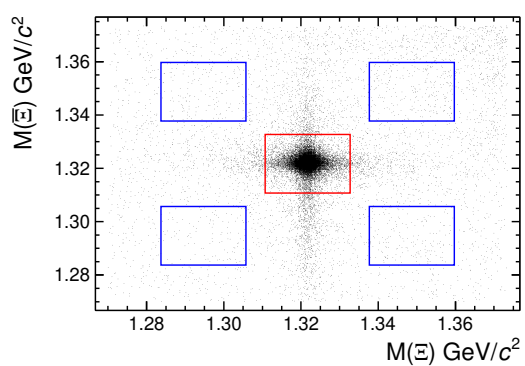


Figure 16: 2012 neutron channel

1 4) Ξ^- invariant mass, 5) $\bar{\Lambda}$ invariant mass, 6) $\cos\theta(\bar{\Xi}^+)$, 7) n invariant mass, 8) the angle between Λ and
 2 γ_1 , 9) the angle between Λ and γ_2 , 10) χ^2 of secondary vertex fit of $\bar{\Xi}^+$, 11) χ^2 of secondary vertex fit of
 3 $\bar{\Lambda}$, 12) χ^2 of kinematic fit. The distributions of other data samples are very similar to the example and
 4 they all have a good agreement between data and corresponding MC simulation. We will leave the rests
 5 in Appendix C.1.

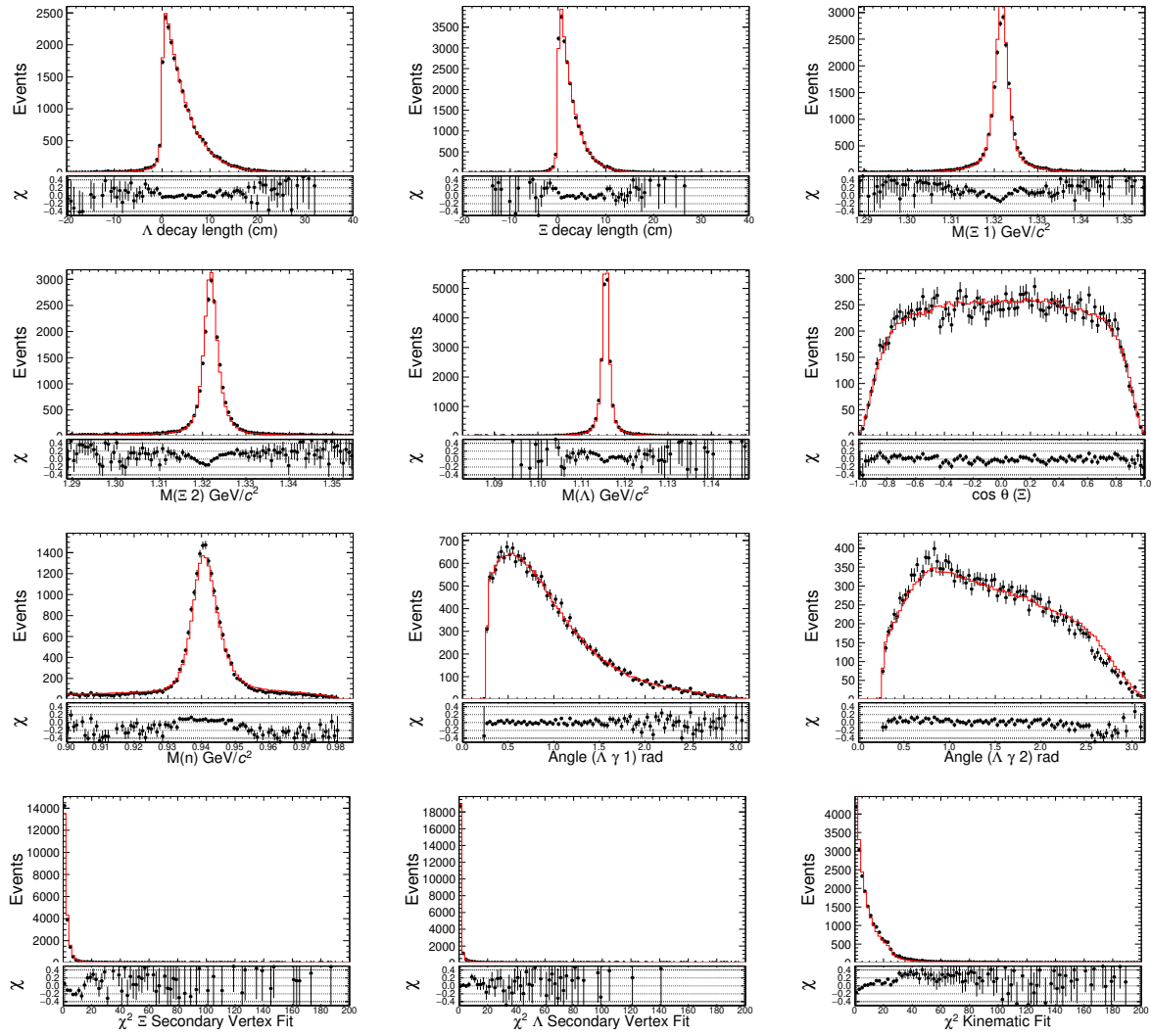


Figure 17: 2012 neutron channel

6 6.4 Transverse momentum and polar angle

7 The transverse momenta and polar angle of the resonance Ξ and Λ and the final states proton, neutron,
 8 charge and neutral pion are also plotted to show that there is no bias. Figure 18 and 19 present the
 9 distributions of transverse momenta and polar angle for the neutron channel in 2012, respectively. All
 10 the particles in decay chain are listed in order 1) $\bar{\Xi}^+$, 2) Ξ^+ , 3) Λ , 4) $\bar{\Lambda}$, 5) proton, 6) neutron, 7) π^+

- 1 from $\bar{\Xi}^+$, 8) π^+ from $\bar{\Lambda}$, 9) π^- from Ξ^- , 10) π^0 , 11) γ_1 , 12) γ_2 . It has to be mentioned that we plot
 2 the distributions of the momentum of π^0 and the energy of γ considering of the independent freedom of
 3 detection. The distributions of the rest data samples can be found in Appendix C.2.

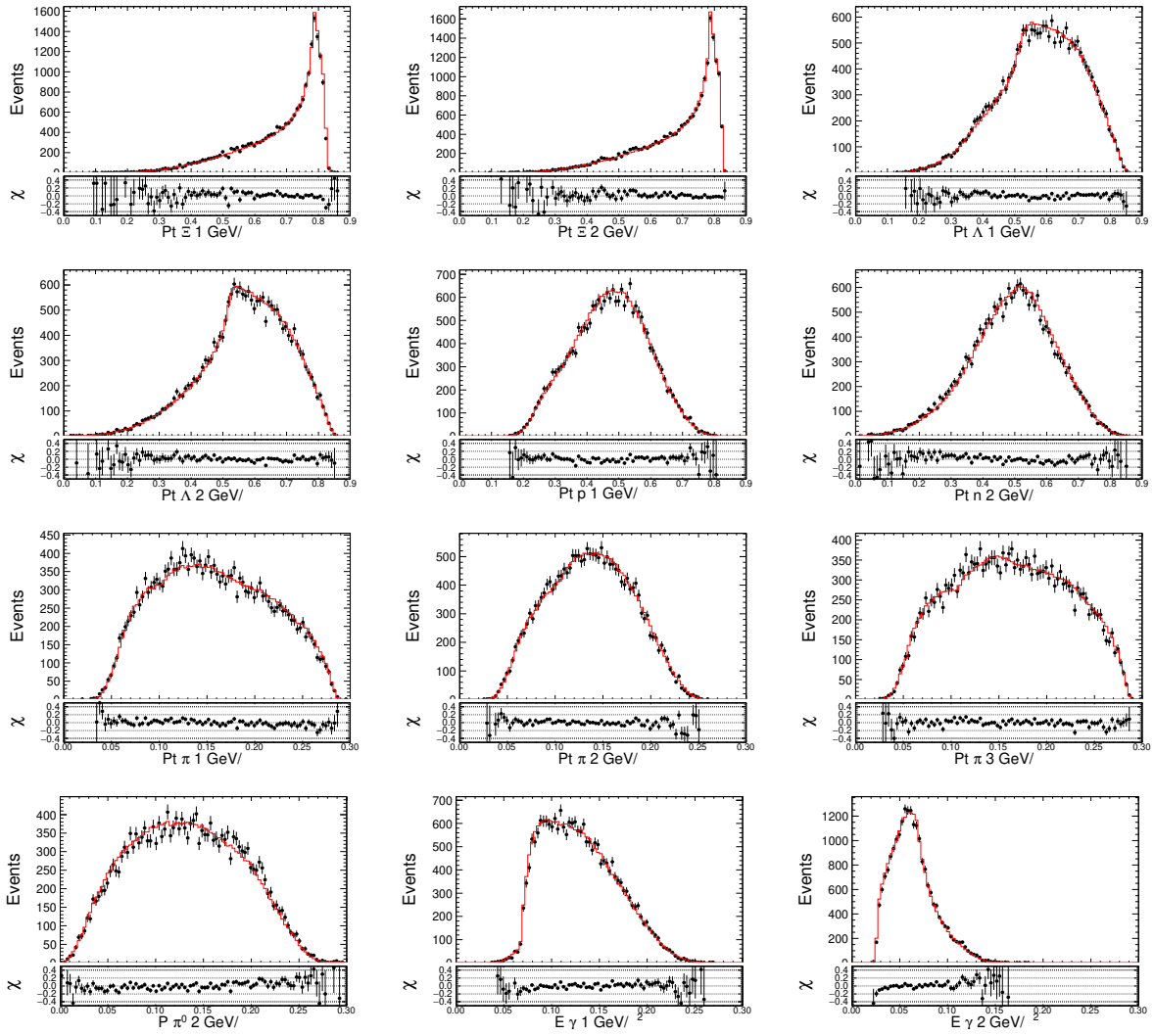


Figure 18: 2012 neutron channel

4 6.5 Polarization and entanglement

5 6.6 Data fit results

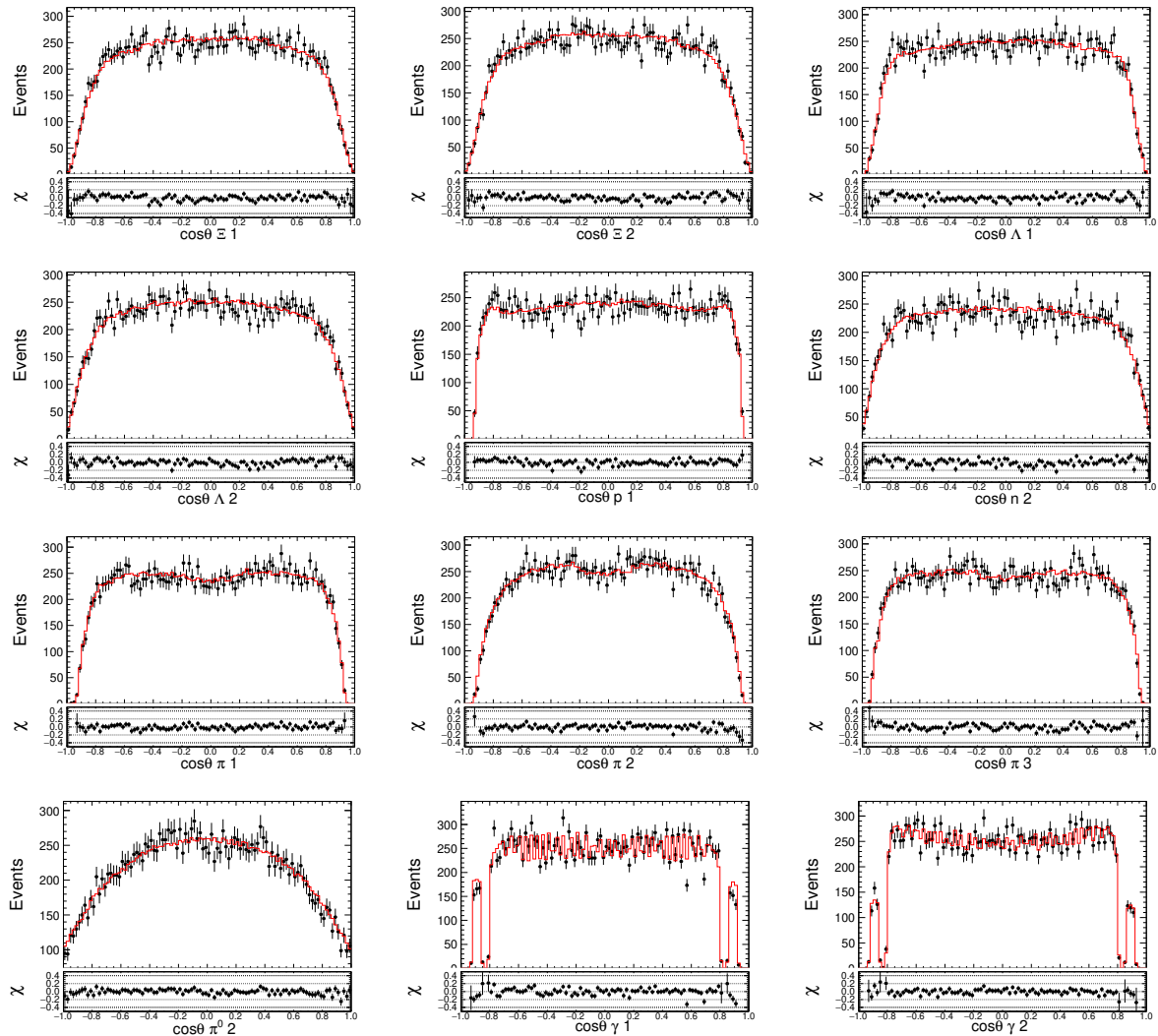


Figure 19: 2012 neutron channel

7 Systematic uncertainty

2 The sources of systematic uncertainties are listed as follows:

- 3 • Reconstruction of Λ : decay length, chi2?
- 4 • Reconstruction of Ξ : decay length, chi2?
- 5 • Reconstruction of π^0 ; chi2? control sample?
- 6 • Reconstruction of π^\pm control sample?
- 7 • Kinematic Fit : chi2 , helix correction
- 8 • Mass cut : barlow test
- 9 • Cos theta cut : barlow test
- 10 • Fitting method :
 - 11 • Mis-combination background : mDIY and sideband
 - 12 • exclusive Background : mDIY and side band

8 Summary

- 2 Based on 567 pb^{-1} of e^+e^- annihilation data collected at $\sqrt{s} = 4.599 \text{ GeV}$ with the BESIII detector
- 3 at the BEPCII, taking advantage of simple clean environment and excellent detector performance, the
- 4 Cabibbo-suppressed decays

1 References

- 2 [1] A. Roodman, eConf **C030908** (2003), TUIT001 [arXiv:physics/0312102 [physics.data-an]].
- 3 [2] M. Ablikim *et al.* [BESIII Collaboration], Nucl. Instrum. Meth. A **614**, 345 (2010).
- 4 [3] C. H. Yu *et al.*, Proceedings of IPAC2016, Busan, Korea, 2016, doi:10.18429/JACoW-IPAC2016-
5 TUYA01.
- 6 [4] M. Ablikim *et al.* [BESIII Collaboration], Chin. Phys. C **44**, 040001 (2020).
- 7 [5] X. Li *et al.*, Radiat. Detect. Technol. Methods **1**, 13 (2017); Y. X. Guo *et al.*, Radiat. Detect.
8 Technol. Methods **1**, 15 (2017); P. Cao *et al.*, Nucl. Instrum. Meth. A **953**, 163053 (2020).
- 9 [6] S. Agostinelli *et al.* [GEANT4 Collaboration], Nucl. Instrum. Meth. A **506**, 250 (2003).
- 10 [7] S. Jadach, B. F. L. Ward and Z. Was, Phys. Rev. D **63**, 113009 (2001); Comput. Phys. Commun.
11 **130**, 260 (2000).
- 12 [8] D. J. Lange, Nucl. Instrum. Meth. A **462**, 152 (2001); R. G. Ping, Chin. Phys. C **32**, 599 (2008).
- 13 [9] cite the reference given in the pdglive:
14 <http://pdglive.lbl.gov/ParticleGroup.action?init=0&node=BXXX040>.
- 15 [10] J. C. Chen, G. S. Huang, X. R. Qi, D. H. Zhang and Y. S. Zhu, Phys. Rev. D **62**, 034003 (2000);
16 R. L. Yang, R. G. Ping and H. Chen, Chin. Phys. Lett. **31**, 061301 (2014).
- 17 [11] E. Richter-Was, Phys. Lett. B **303**, 163 (1993).
- 18 [12] Y. Kohara, Nuovo Cim. **A111**, 67 (1998).
- 19 [13] M. A. Ivanov, J. G. Korner, V. E. Lyubovitskij, A. G. Rusetsky Phys. Rev. **D57**, 5632 (1998).
- 20 [14] K. K. Sharma, R. C. Verma Phys. Rev. **D55**, 7067 (1997).
- 21 [15] T. Uppal, R. C. Verna, M. P. Khanna Phys. Rev. **D49**, 3417 (1994).
- 22 [16] P. Zenczykowski, Phys. Rev. **D50**, 402 (1994).
- 23 [17] J. G. Korner, M. Kramer, Z. Phys. **C55**, 659 (1992).
- 24 [18] J. G. Korner, M. Kramer, J. Willrodt, Z. Phys. **C2**, 117 (1979).
- 25 [19] G. S. Abrams *et al.* (MARKIII Collaboration), Phys. Rev. Lett. **44**, 10 (1980).

- ¹ [20] A. M. Cnops *et al.* (BNL-0427 Collaboration), Phys. Rev. Lett. **42**, 197 (1979).
- ² [21] K. A. Olive *et al.* (Particle Data Group), Chin. Phys. **C38**, 090001 (2014).
- ³ [22] M. Ablikim *et al.* (BESIII Collaboration), Phys. Rev. Lett. **116**, 052001 (2016).
- ⁴ [23] A. Zupanc *et al.* (Belle Collaboration), Phys. Rev. Lett. **113**, 042002 (2014).
- ⁵ [24] M. Ablikim *et al.* (BESIII Collaboration), Chin. Phys.. **C39**, 093001 (2015). (arXiv:1503.03408)
- ⁶ [25] M. Ablikim *et al.* (BESIII Collaboration), Nucl. Instrum. Meth. A **614**, 345 (2010).
- ⁷ [26] J. Z. Bai *et al.* (BES Collaboration), Nucl. Instrum. Meth. A **344**, 319 (1994).
- ⁸ [27] D. M. Asner *et al.*, Int. Journal of Mod. Phys. A **24**, 1 (2009). (arXiv:0809.1869).
- ⁹ [28] S. Jadach, B. F. L. Ward, Z. Was, Phys. Rev. D **63**, 113009 (2001); Comput. Phys. Commun. 130,
¹⁰ 260 (2000).
- ¹¹ [29] E. Barberio and Z. Was, Comput. Phys. Commun. **79**, 291 (1994).
- ¹² [30] R. G. Ping, Chin. Phys. C **32**, 599 (2008).
- ¹³ [31] D. J. Lange, Nucl. Instrum. Meth. A **462**, 152 (2001).
- ¹⁴ [32] J. C. Chen, G. S. Huang, X. R. Qi, D. H. Zhang and Y. S. Zhu, Phys. Rev. D **62**, 034003 (2000).
- ¹⁵ [33] S. Agostinelli *et al.* (GEANT Collaboration), Nucl. Instrum. Meth. A **506**, 250 (2003).
- ¹⁶ [34] J. Allison *et al.*, IEEE Trans. Nucl. Sci. **53**, 270 (2006).
- ¹⁷ [35] Z. Y. Deng *et al.*, Chin. Phys. C **30**, 371 (2006).
- ¹⁸ [36] W. P. Wang *et al.*, bes3 memo "Cross section measurement of $e^+e^- \rightarrow \Lambda_c^+\bar{\Lambda}_c^-$ near threshold with
¹⁹ BESIII".
- ²⁰ [37] H. Albrecht *et al.* (ARGUS Collaboration), Phys. Rev. Lett. B **241**, 278 (1990).
- ²¹ [38] G. Pakhlova *et al.* (Belle Collaboration), Phys. Rev. Lett. **101** (2008) 172001. (arXiv:0807.4458).
- ²² [39] R.M.Baltrusaitis *et al.* (MARK-III Collaboration), Phys. Rev. Lett. **56**, 2140 (1986).
- ²³ [40] J. Adler *et al.* (MARK-III Collaboration), Phys. Rev. Lett. **60**, 89 (1988).
- ²⁴ [41] S. U. Chung, Phys. Rev. D **57**, 431 (1998).

Appendices

1 A True information

- 2 In order to have an overall impression of the distribution of momentums of the final states and 16 moments, the true information are plotted to provide reference for the determination of selection conditions.
- 3 We plot the distributions for 2009, 2012, 2018, and 2019 samples separately. The statistic for each sample is 30 times larger than the corresponding data sample.

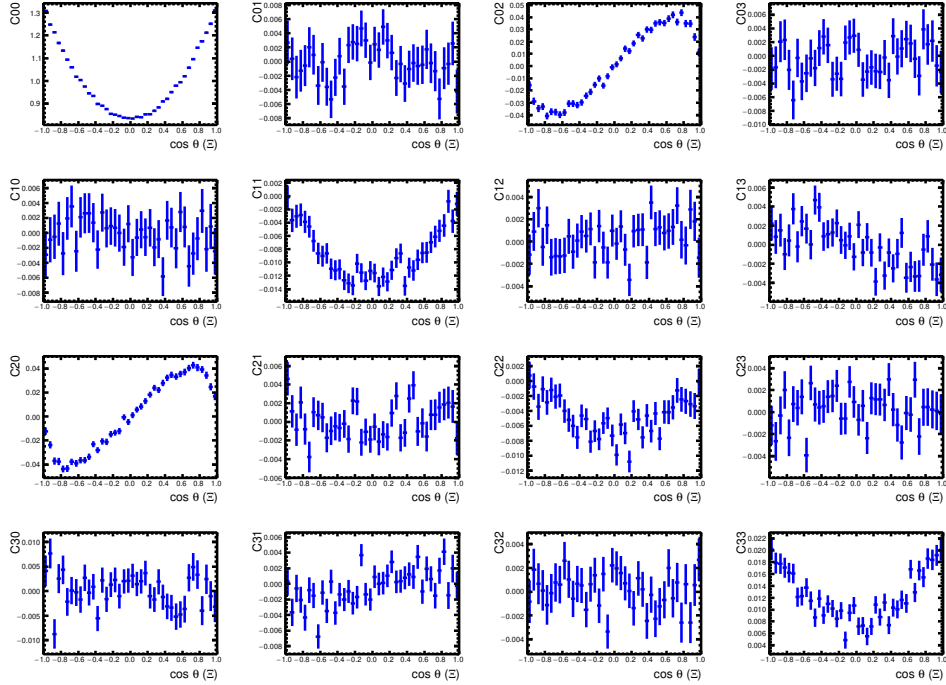


Figure 20: Using 2009 mDIY MC as example to show the true distributions of the 16 moments of neutron channel for $J/\psi \rightarrow \Xi^- \bar{\Xi}^+$.

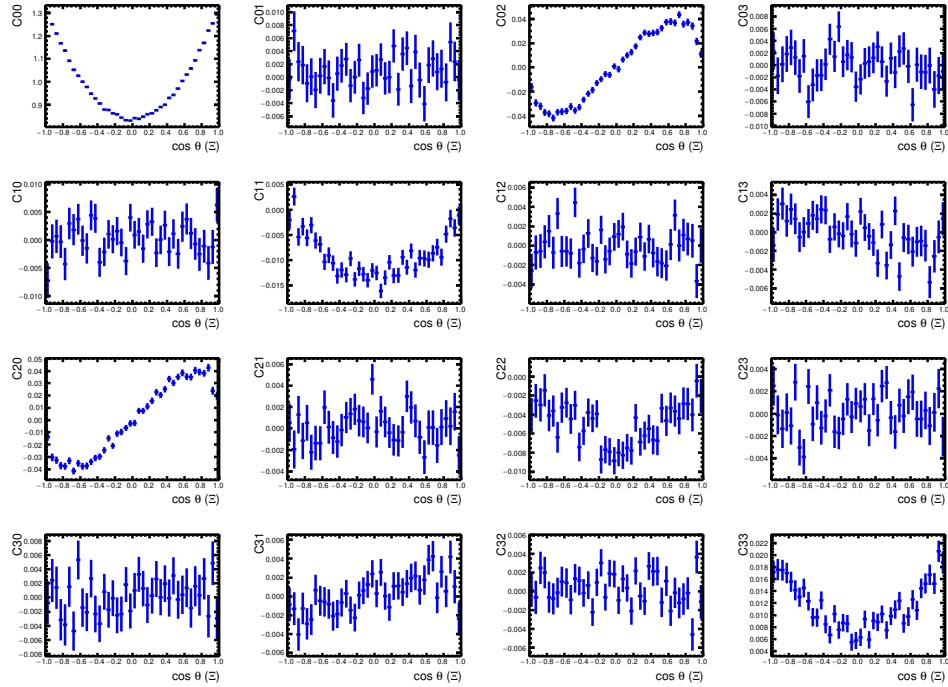


Figure 21: Using 2009 mDIY MC as example to show the true distributions of the 16 moments of anti-neutron channel for $J/\psi \rightarrow \Xi^- \bar{\Xi}^+$.

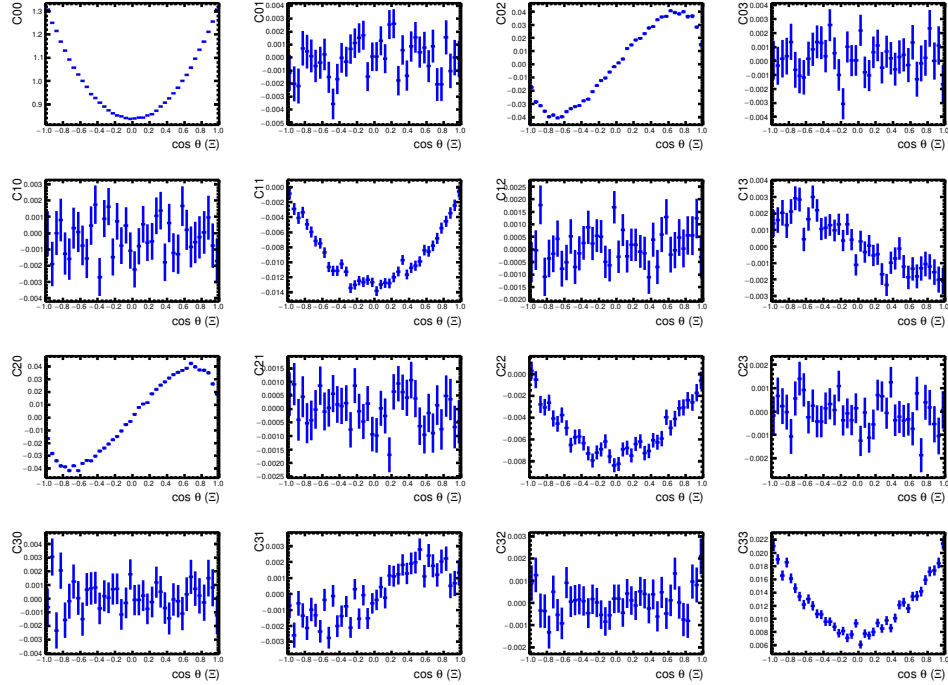


Figure 22: Using 2012 mDIY MC as example to show the true distributions of the 16 moments of neutron channel for $J/\psi \rightarrow \Xi^- \bar{\Xi}^+$.

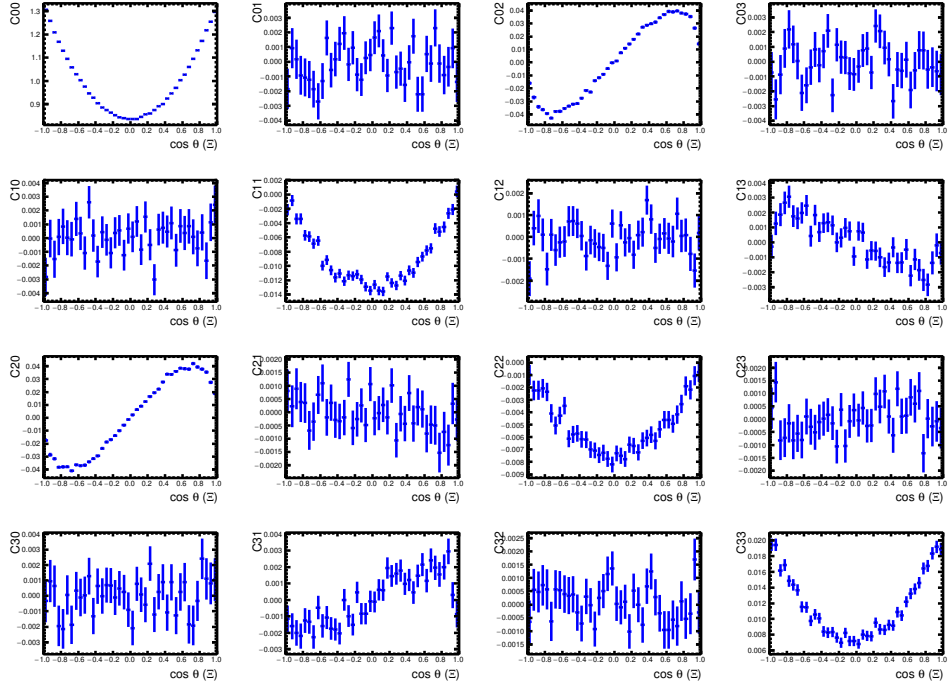


Figure 23: Using 2012 mDIY MC as example to show the true distributions of the 16 moments of anti-neutron channel for $J/\psi \rightarrow \Xi^- \bar{\Xi}^+$.

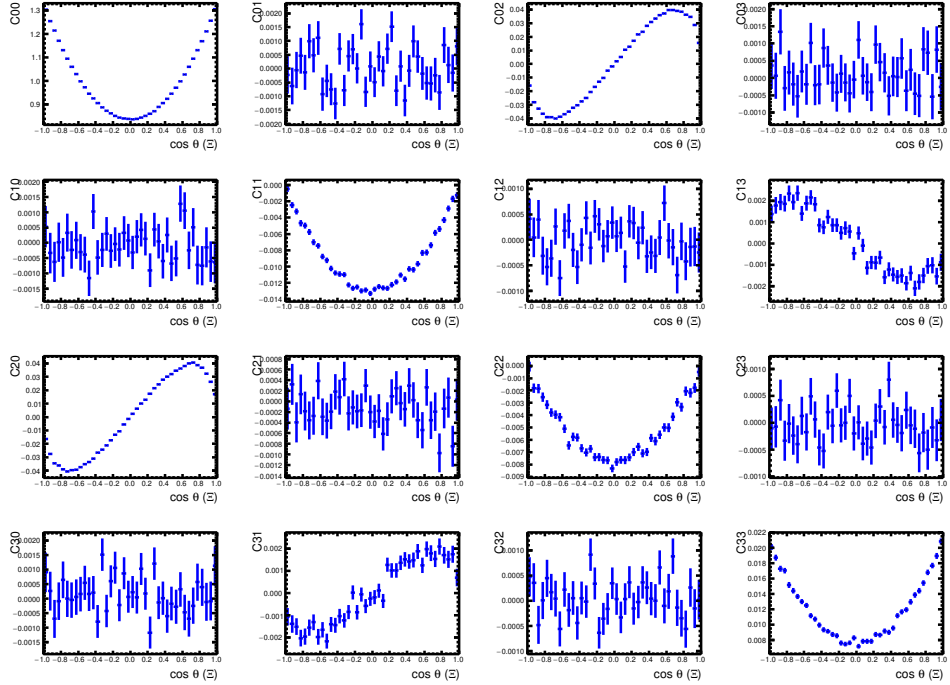


Figure 24: Using 2018 mDIY MC as example to show the true distributions of the 16 moments of neutron channel for $J/\psi \rightarrow \Xi^- \bar{\Xi}^+$.

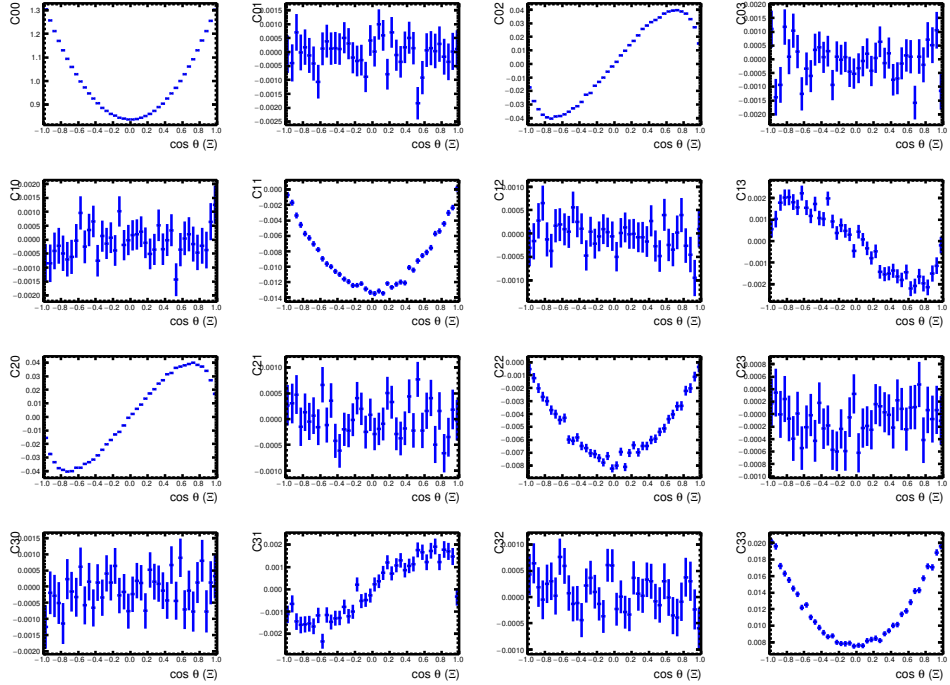


Figure 25: Using 2018 mDIY MC as example to show the true distributions of the 16 moments of anti-neutron channel for $J/\psi \rightarrow \Xi^- \bar{\Xi}^+$.

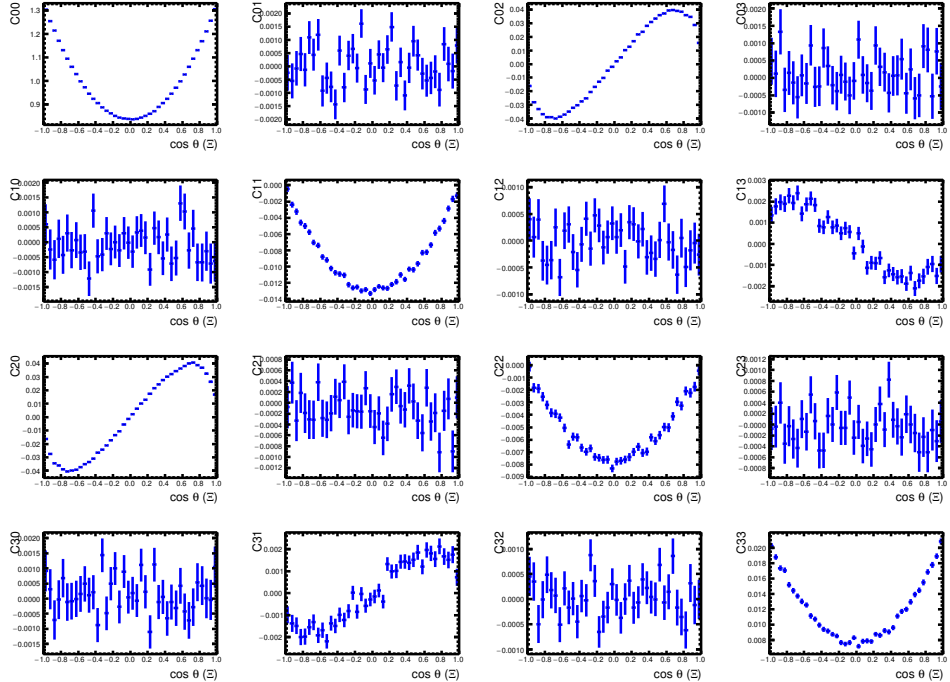


Figure 26: Using 2019 mDIY MC as example to show the true distributions of the 16 moments of neutron channel for $J/\psi \rightarrow \Xi^- \bar{\Xi}^+$.

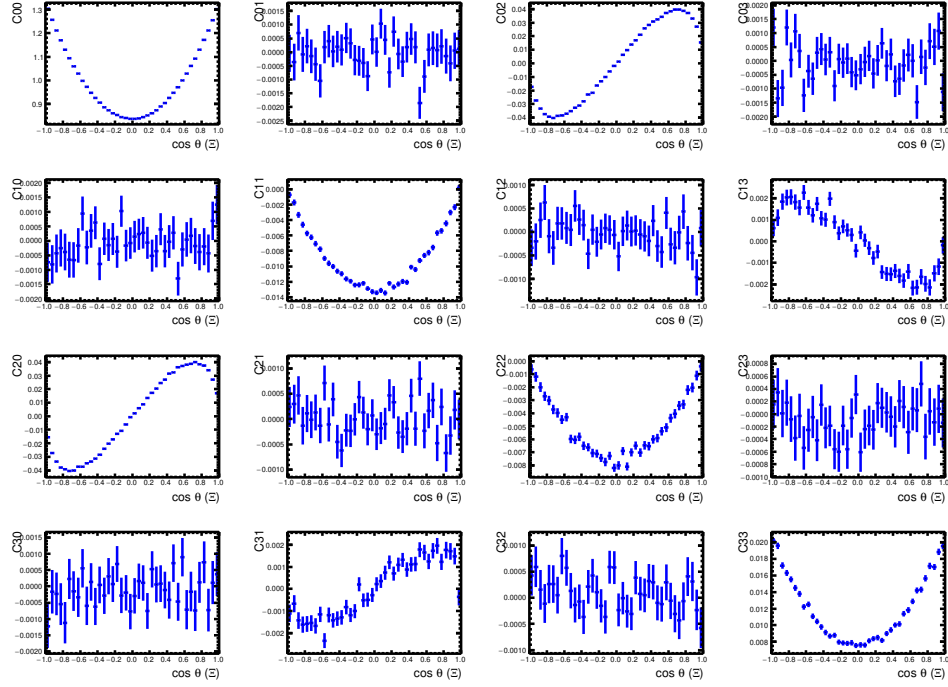


Figure 27: Using 2019 mDIY MC as example to show the true distributions of the 16 moments of anti-neutron channel for $J/\psi \rightarrow \Xi^- \bar{\Xi}^+$.

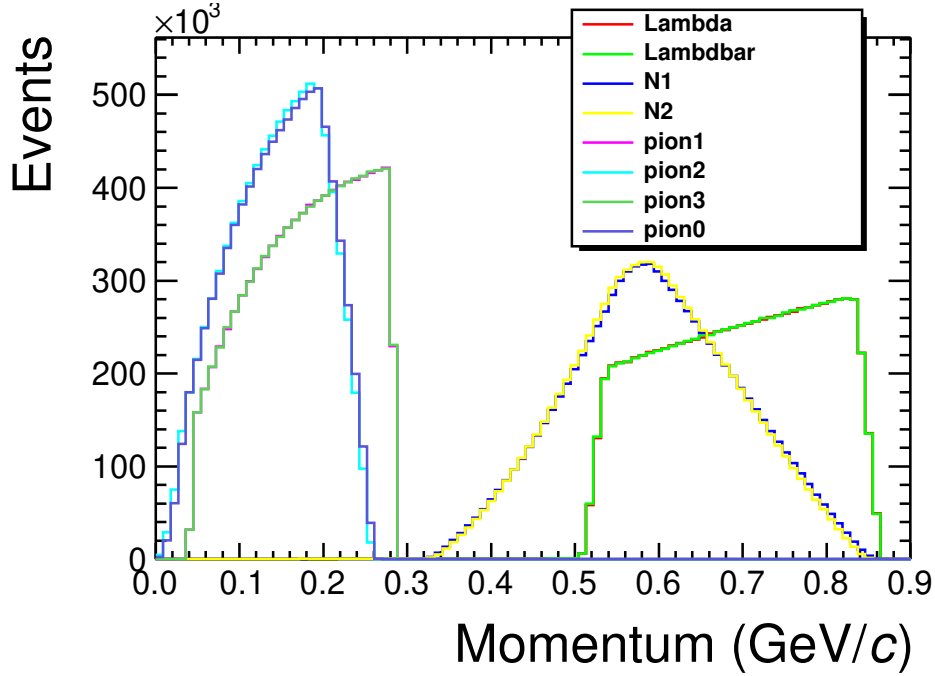


Figure 28: Using 2012 mDIY MC as example to show the true momentum of final states and Λ resonances in neutron channel for $J/\psi \rightarrow \Xi^- \bar{\Xi}^+$. The order of final states in legend is Λ , $\bar{\Lambda}$, n , \bar{p} , π_Ξ^+ , π_Λ^+ , π_Ξ^- , and π^0 .

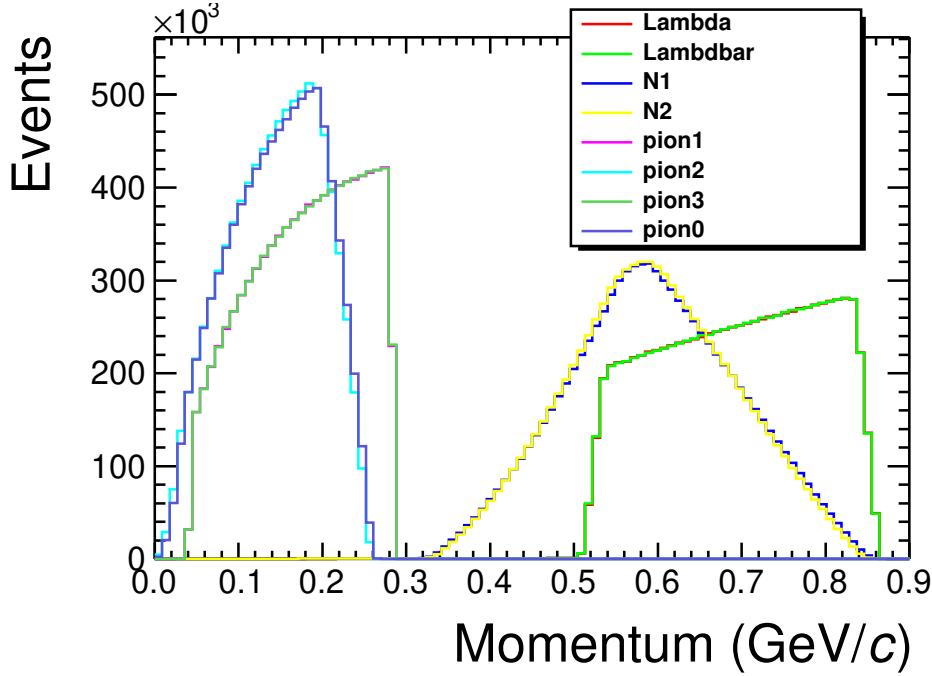


Figure 29: Using 2012 mDIY MC as example to show the true momentum of final states and Λ resonances in anti-neutron channel for $J/\psi \rightarrow \Xi^-\bar{\Xi}^+$. The order of final states in legend is Λ , $\bar{\Lambda}$, p , \bar{n} , π_Ξ^- , π_Λ^- , π_Ξ^+ , and π^0 .

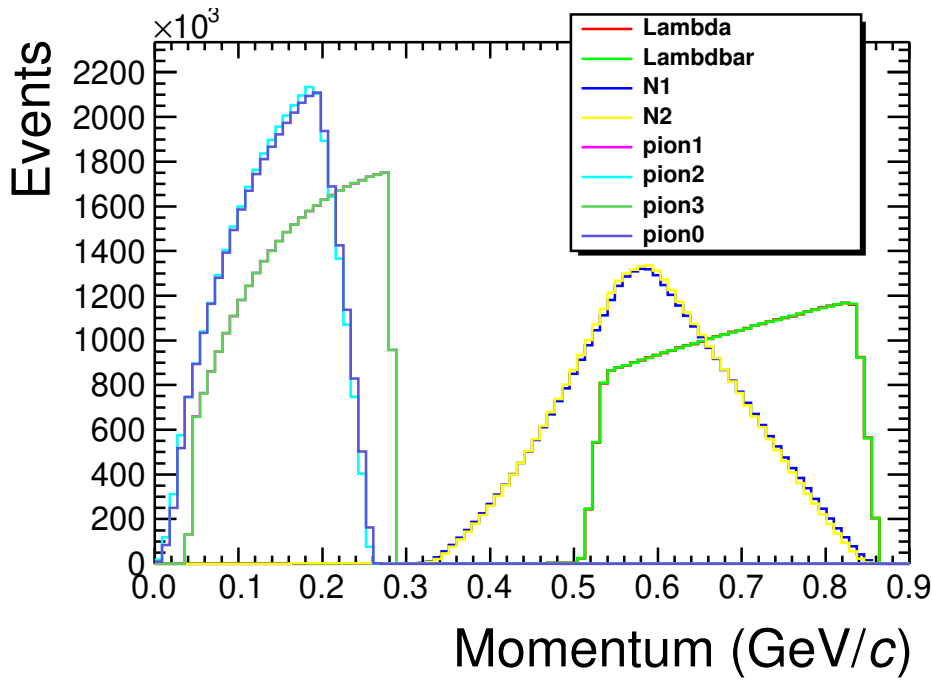


Figure 30: Using 2018 mDIY MC as example to show the true momentum of final states and Λ resonances in neutron channel for $J/\psi \rightarrow \Xi^-\bar{\Xi}^+$. The order of final states in legend is Λ , $\bar{\Lambda}$, n , \bar{p} , π_Ξ^+ , π_Λ^+ , π_Ξ^- , and π^0 .

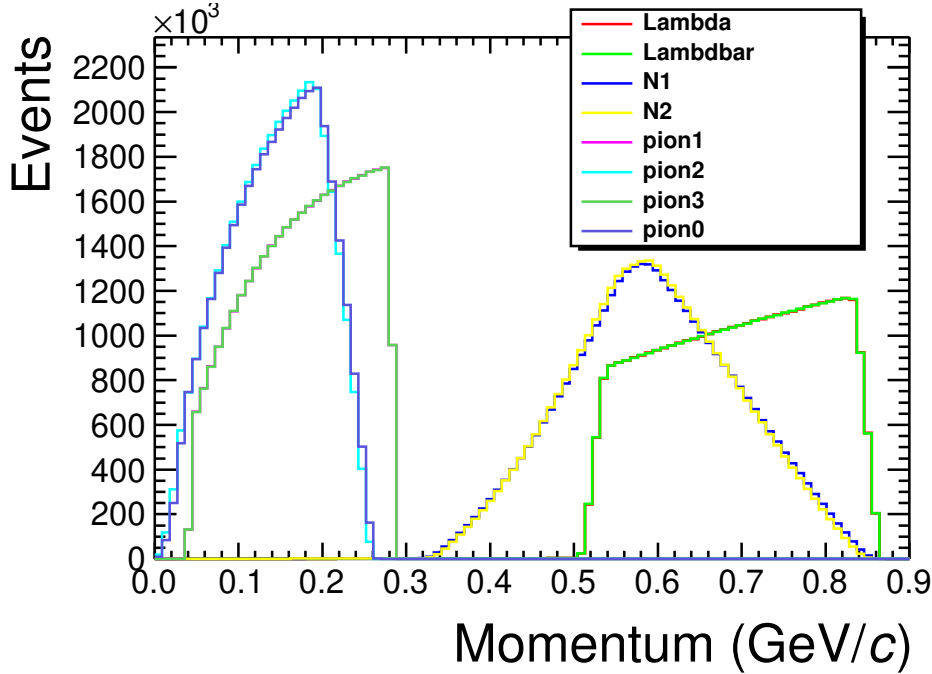


Figure 31: Using 2018 mDIY MC as example to show the true momentum of final states and Λ resonances in anti-neutron channel for $J/\psi \rightarrow \Xi^-\bar{\Xi}^+$. The order of final states in legend is Λ , $\bar{\Lambda}$, p , \bar{n} , π_Ξ^- , π_Λ^- , π_Ξ^+ , and π^0 .

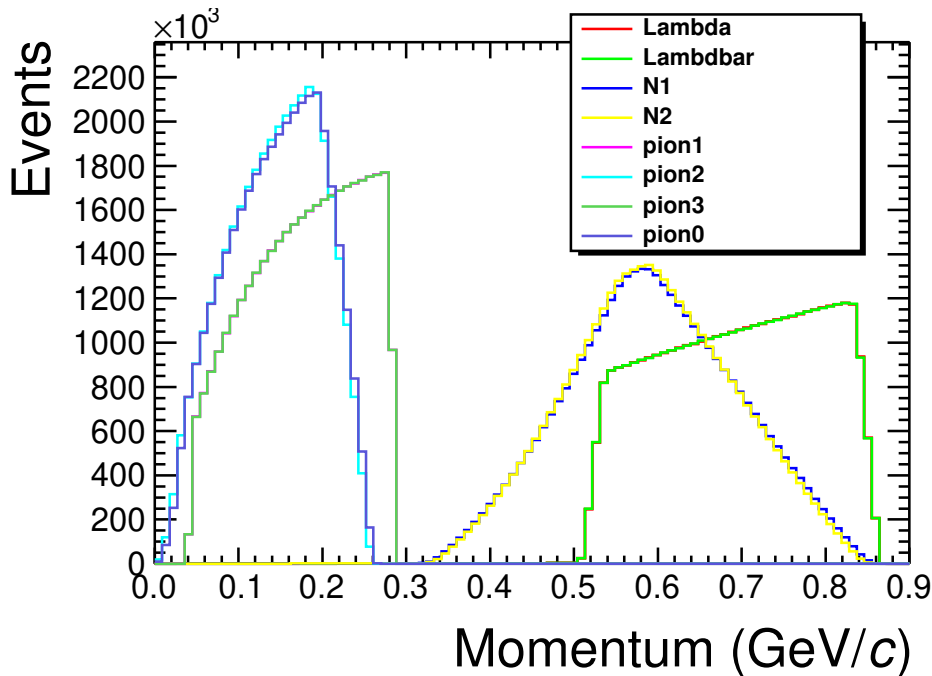


Figure 32: Using 2019 mDIY MC as example to show the true momentum of final states and Λ resonances in neutron channel for $J/\psi \rightarrow \Xi^-\bar{\Xi}^+$. The order of final states in legend is Λ , $\bar{\Lambda}$, n , \bar{p} , π_Ξ^+ , π_Λ^+ , π_Ξ^- , and π^0 .

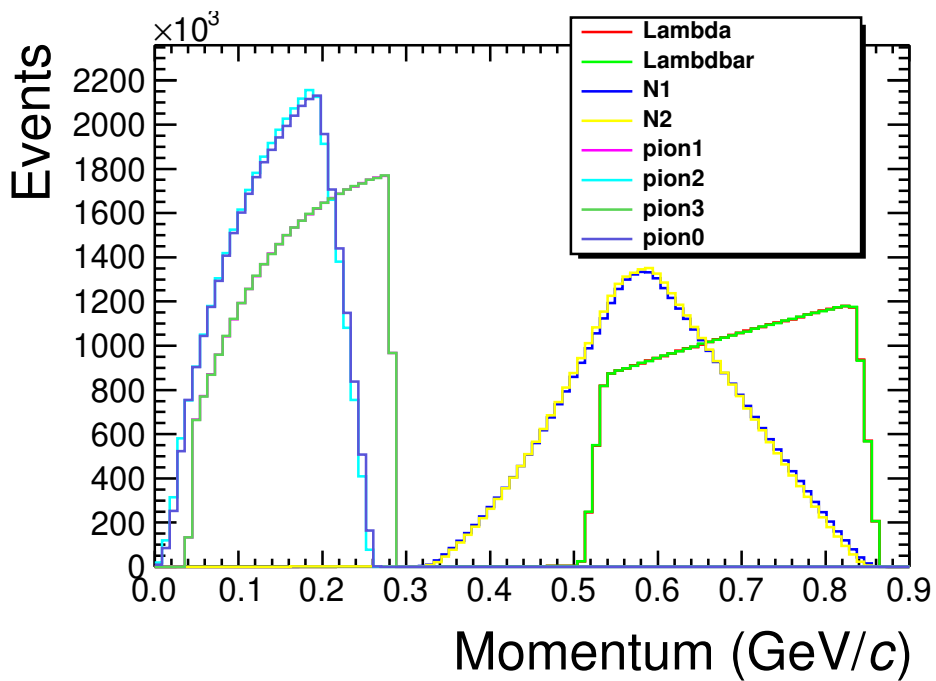


Figure 33: Using 2019 mDIY MC as example to show the true momentum of final states and Λ resonances in anti-neutron channel for $J/\psi \rightarrow \Xi^- \bar{\Xi}^+$. The order of final states in legend is Λ , $\bar{\Lambda}$, p , \bar{n} , π_{Ξ}^- , π_{Λ}^- , π_{Ξ}^+ , and π^0 .

1 B Branch fraction check

1 C Comparison between data and MC

2 C.1 Variables comparison

3 35,17,37.

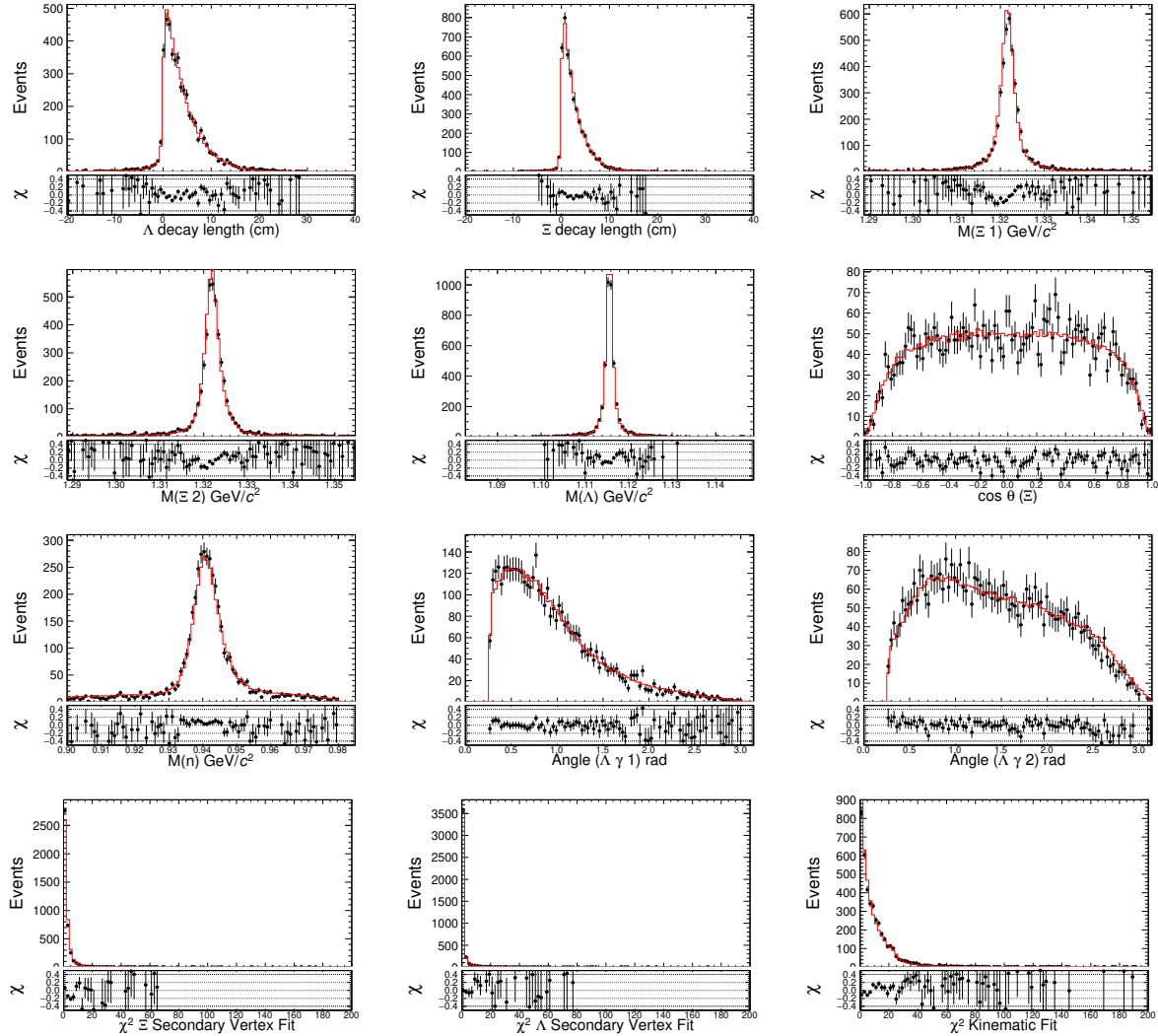


Figure 34: 2009 neutron channel

4 C.2 Transverse momentum and polar angle

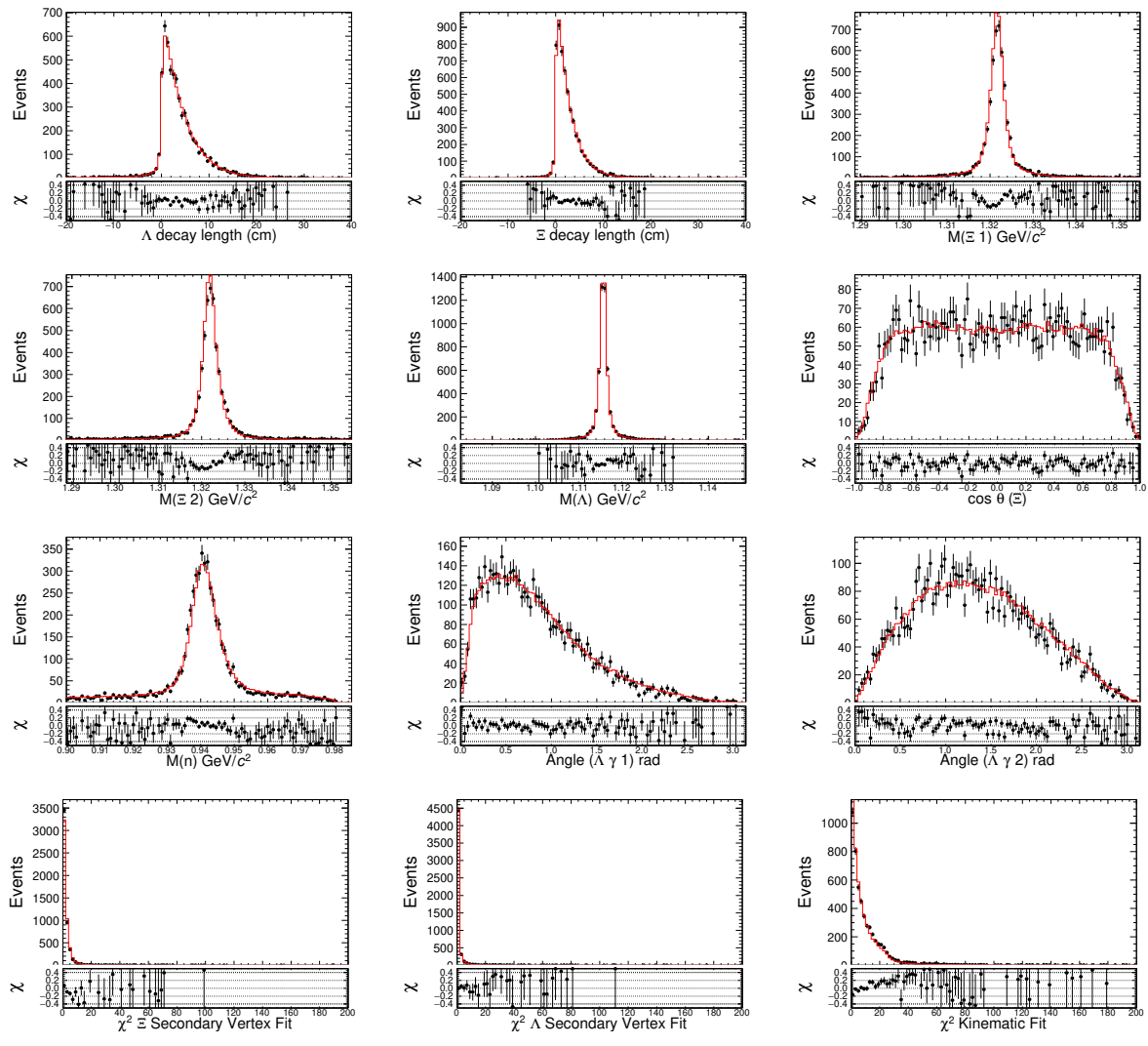


Figure 35: 2009 anti-neutron channel

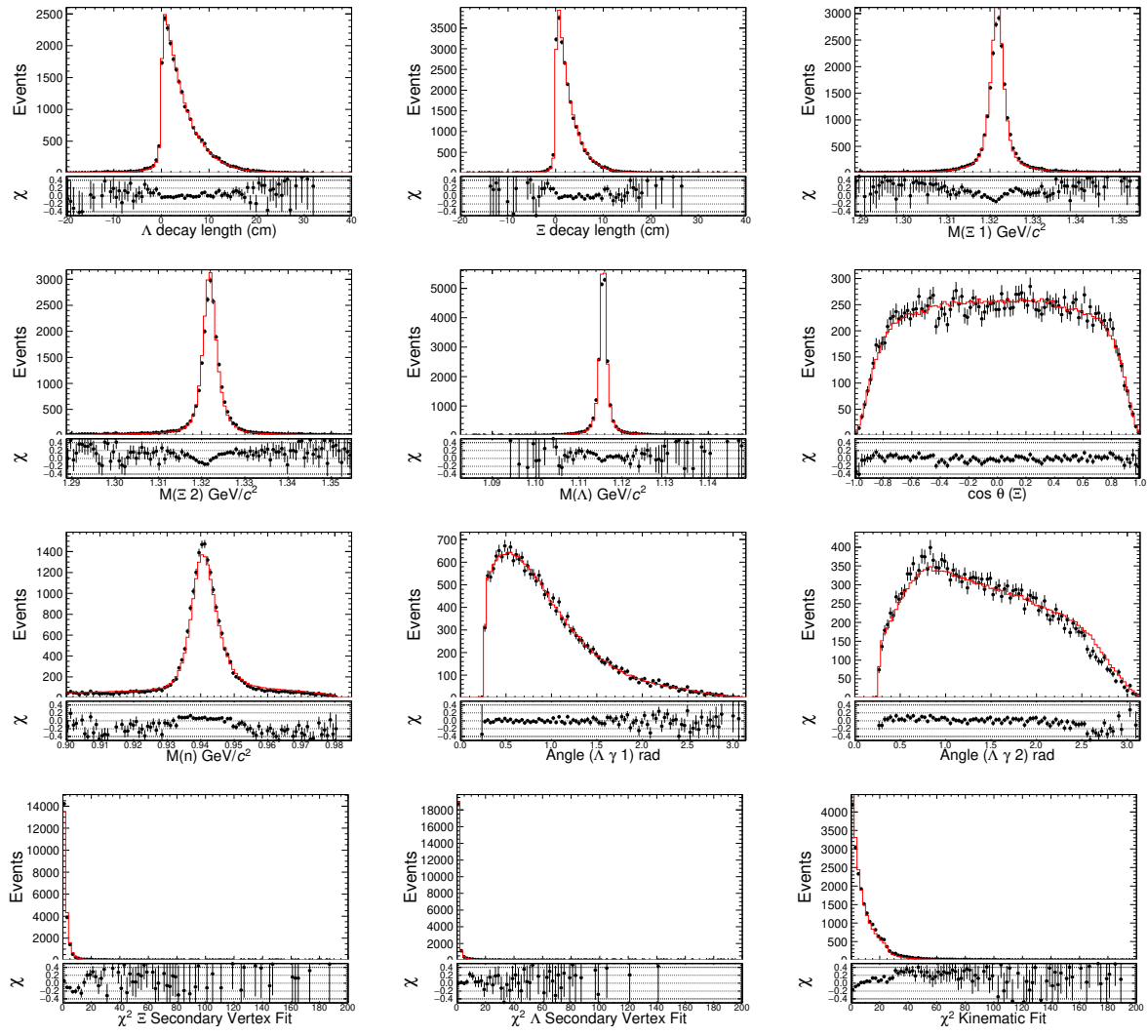


Figure 36: 2012 neutron channel

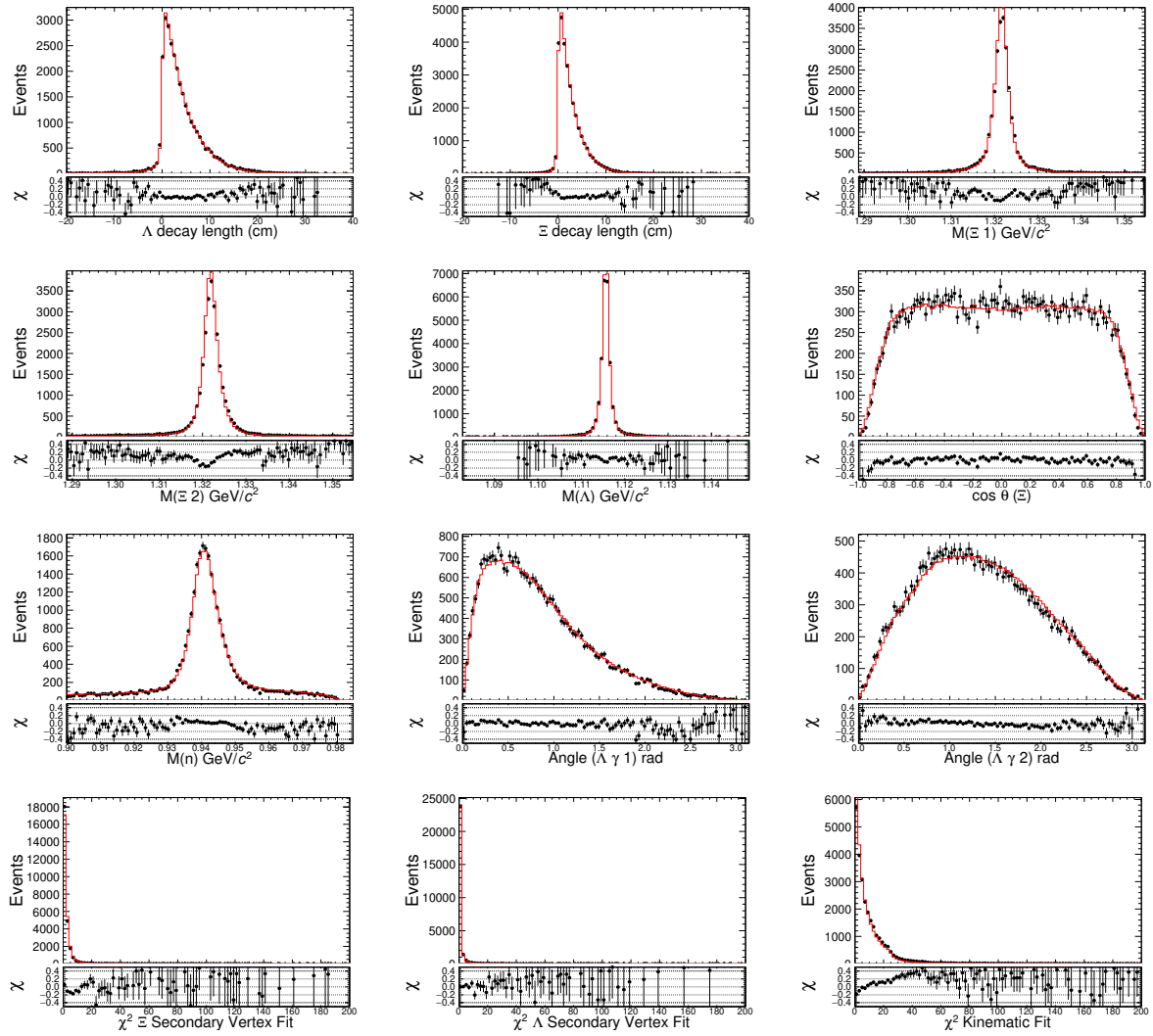


Figure 37: 2012 anti-neutron channel

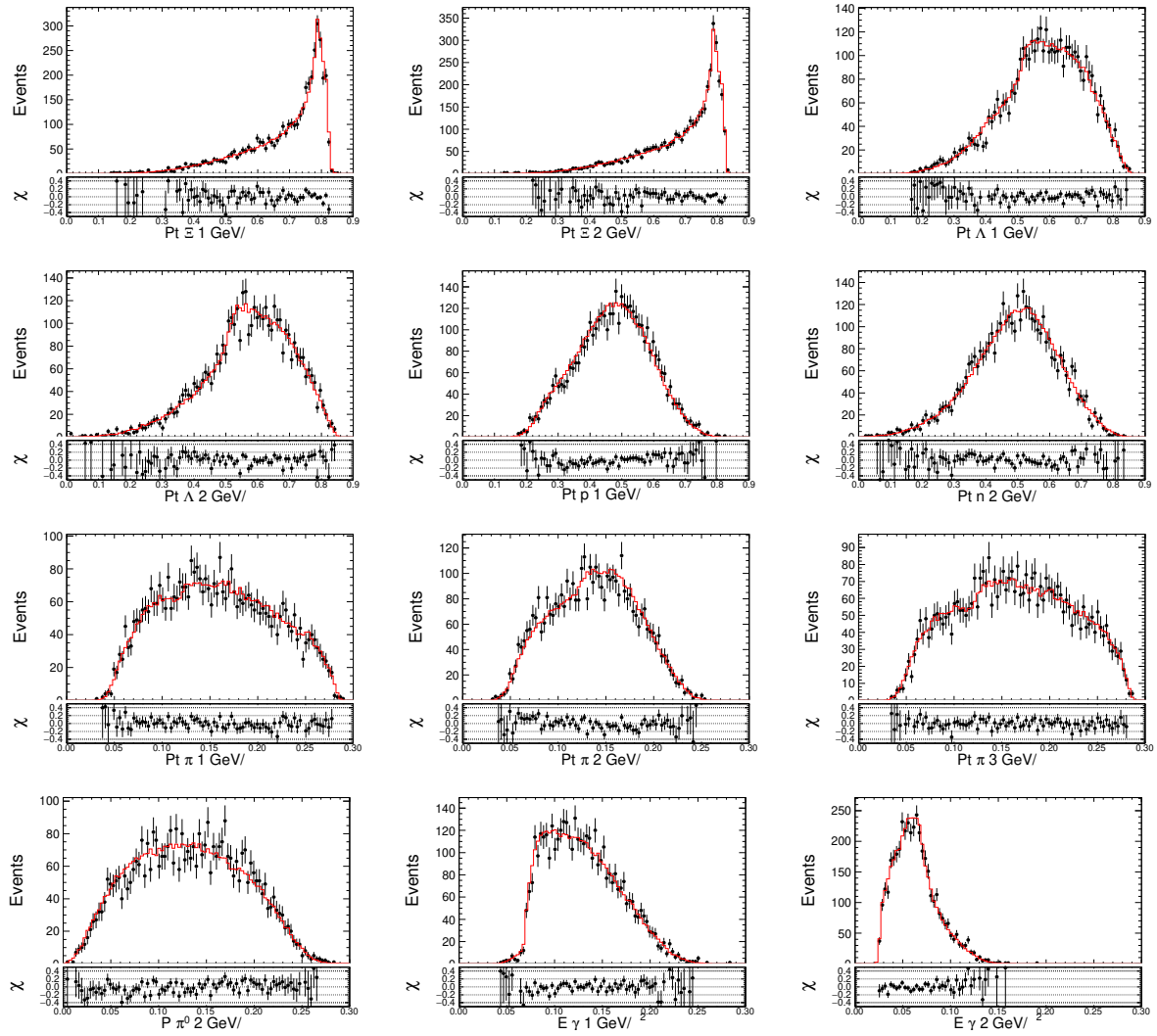


Figure 38: 2009 neutron channel

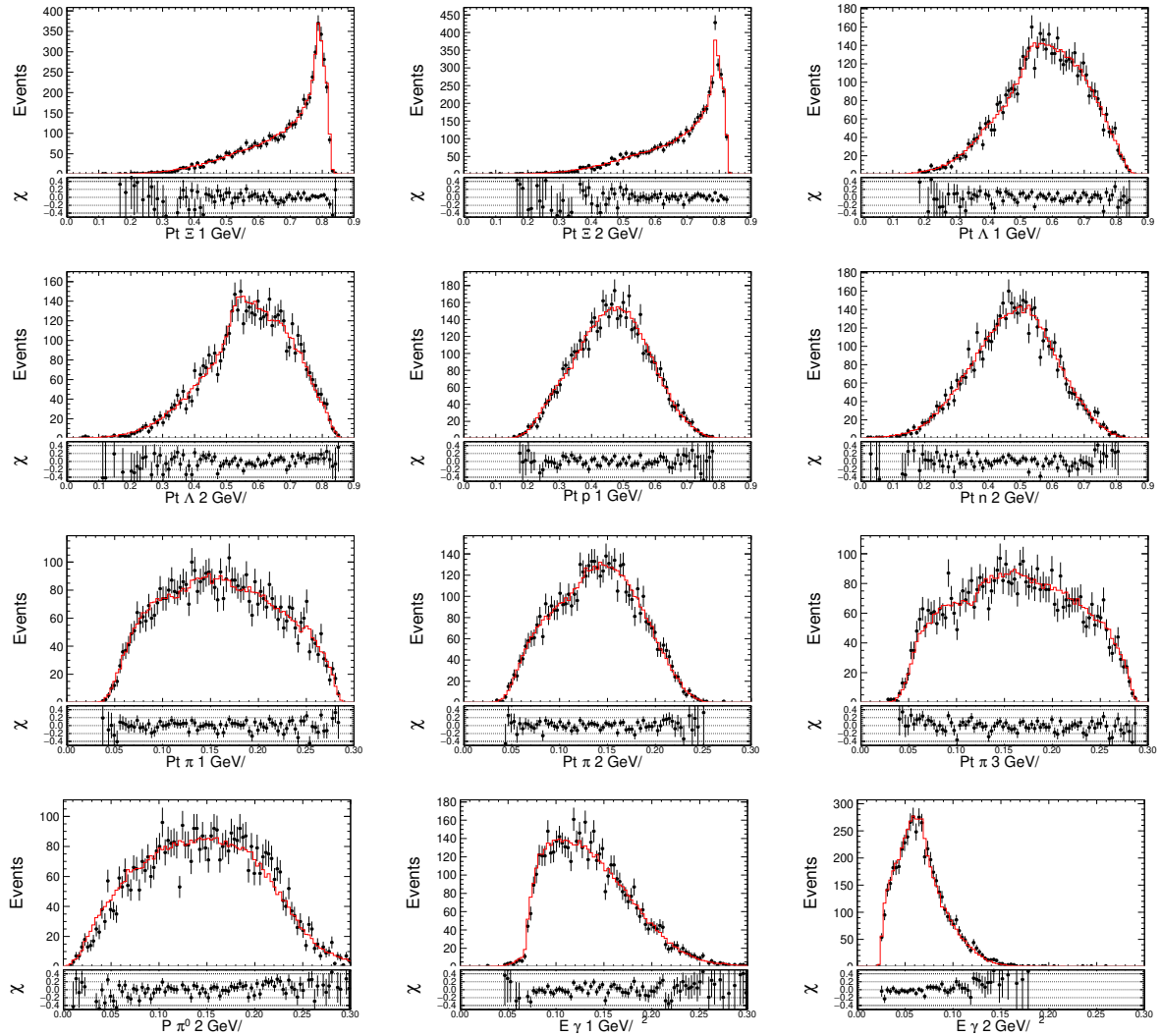


Figure 39: 2009 anti-neutron channel

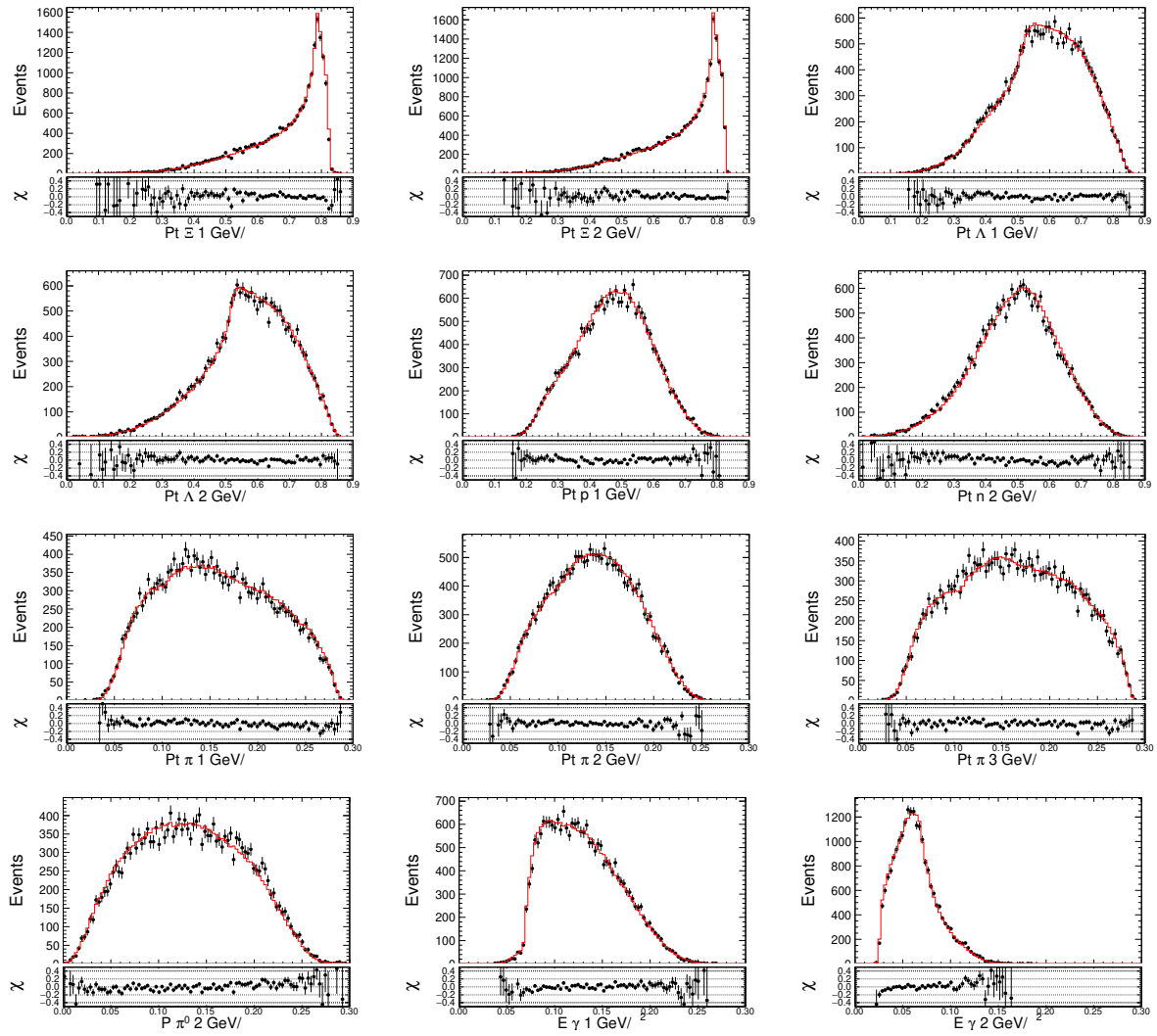


Figure 40: 2012 neutron channel

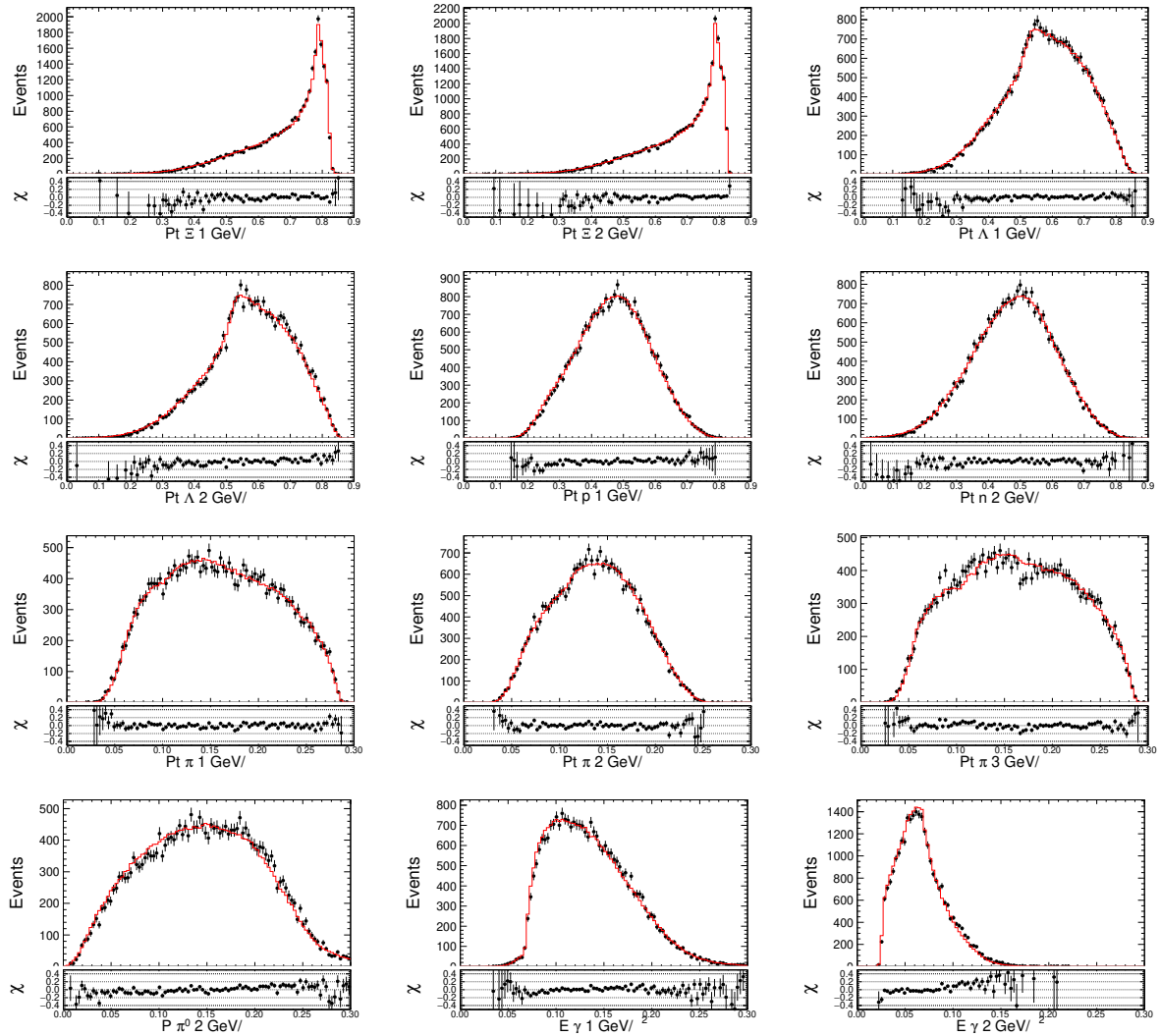


Figure 41: 2012 anti-neutron channel

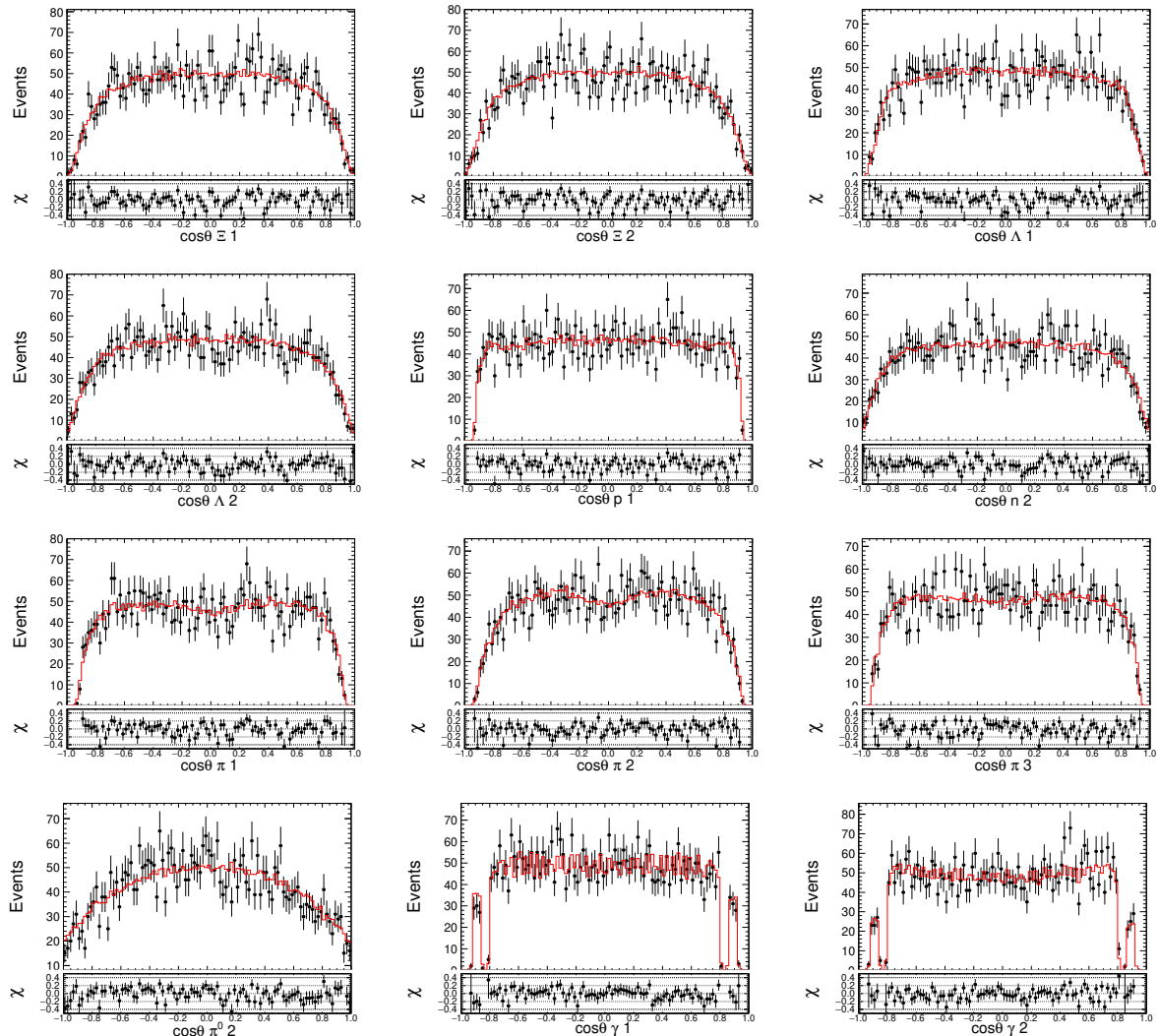


Figure 42: 2009 neutron channel

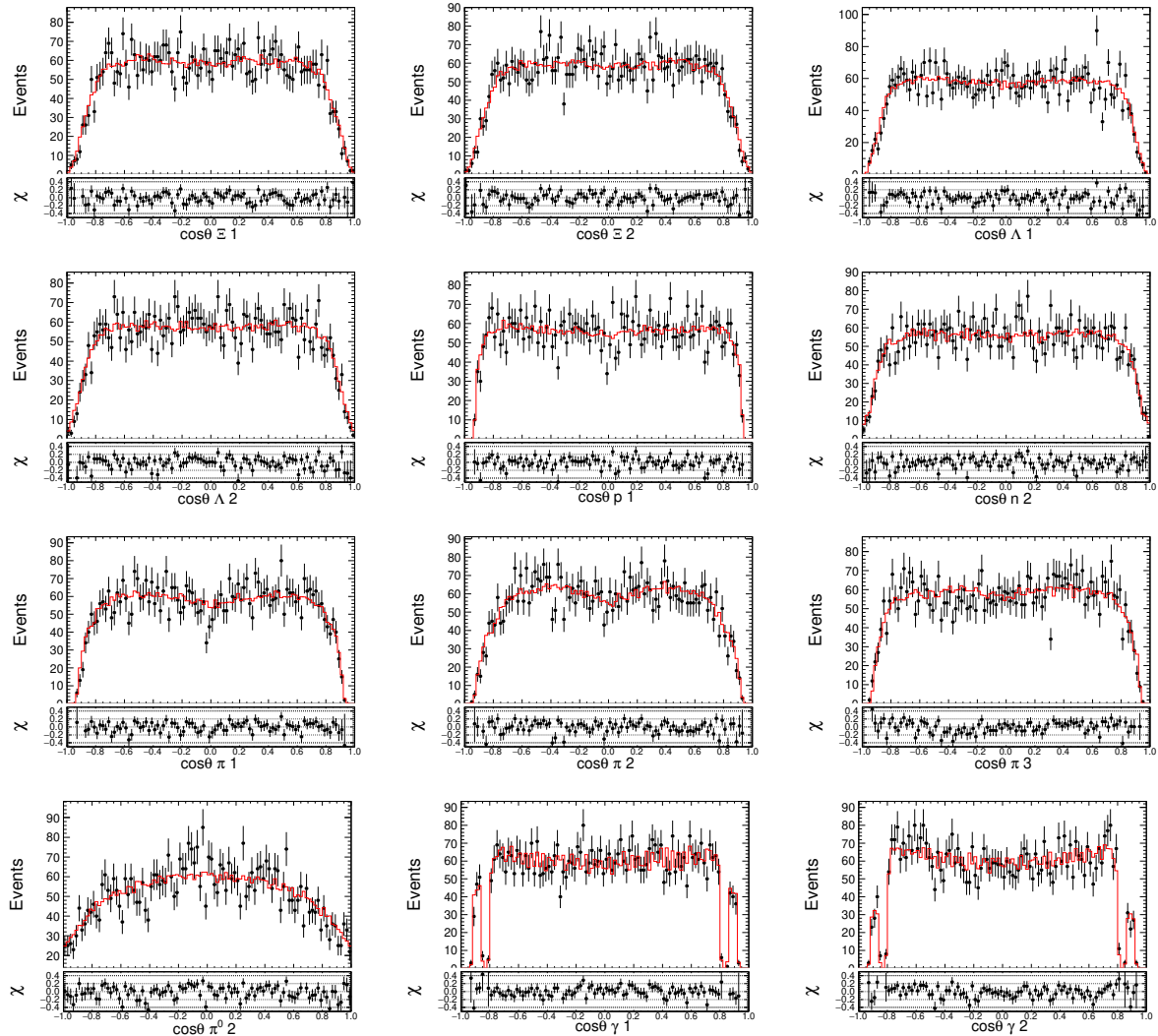


Figure 43: 2009 anti-neutron channel

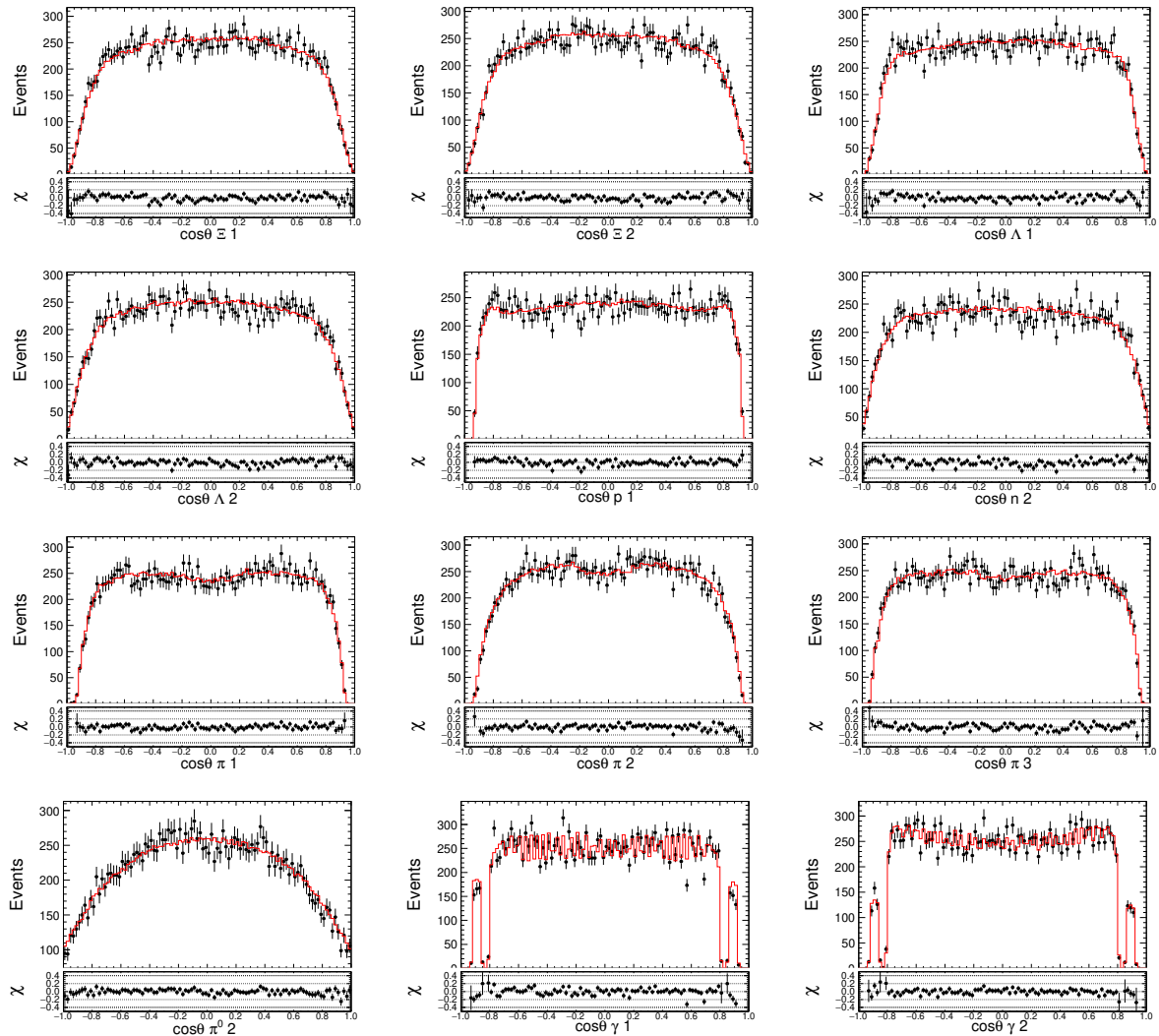


Figure 44: 2012 neutron channel

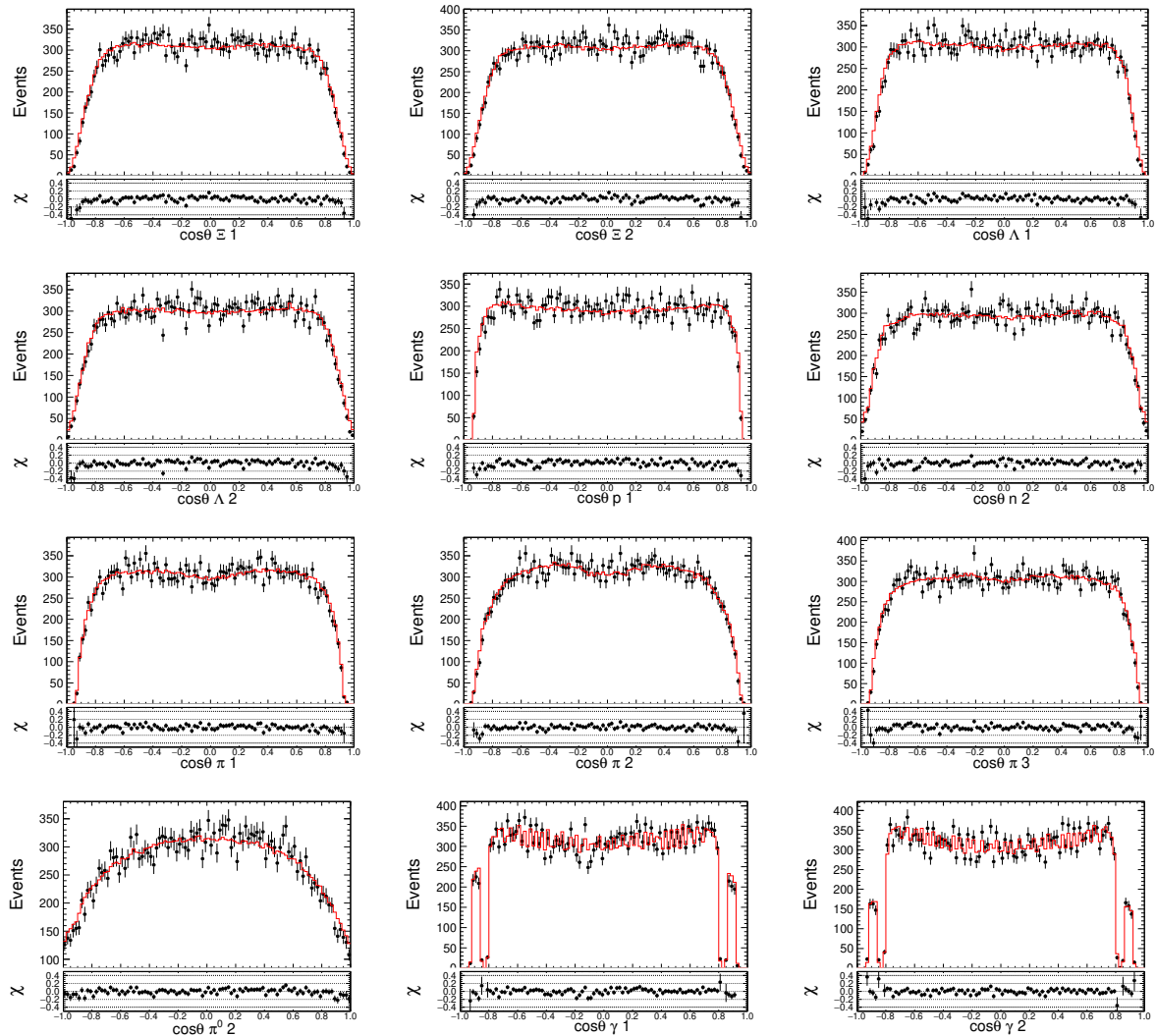


Figure 45: 2012 anti-neutron channel

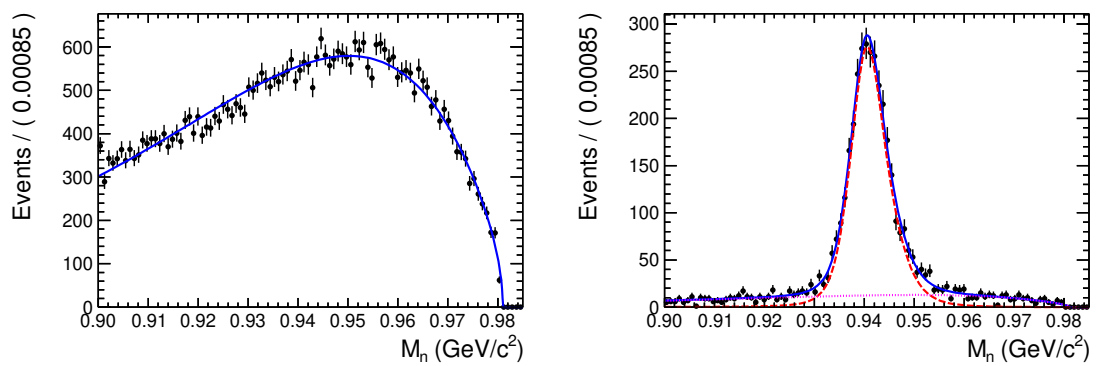


Figure 46: 2009 neutron channel

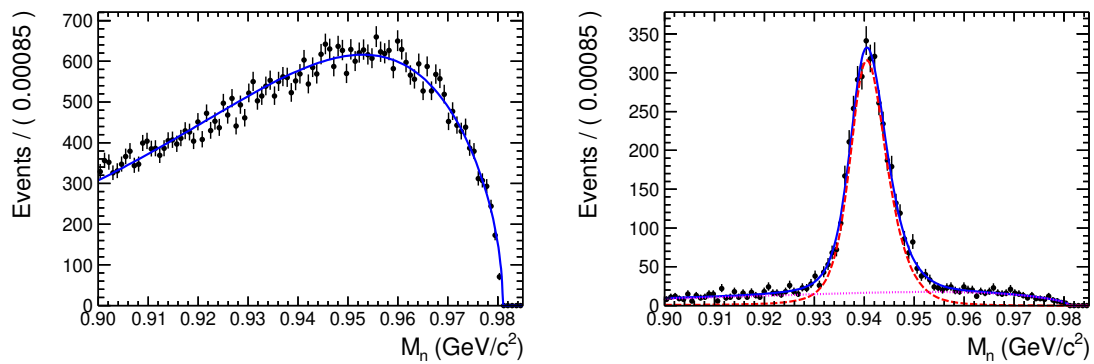


Figure 47: 2009 neutron channel

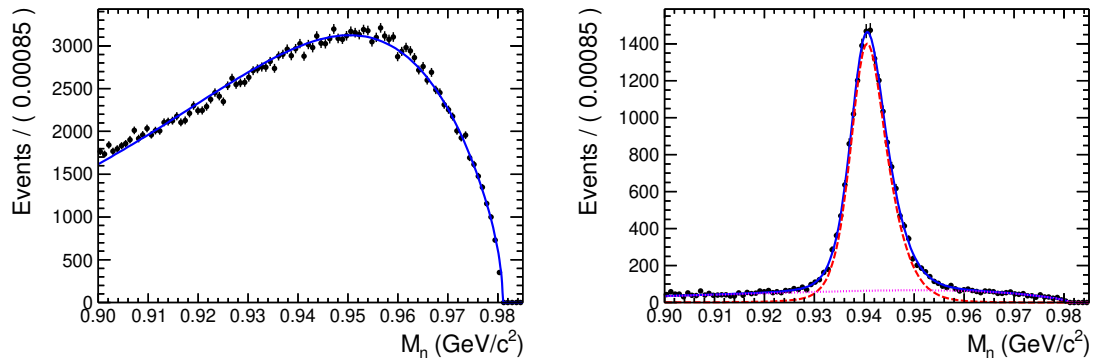


Figure 48: 2012 neutron channel

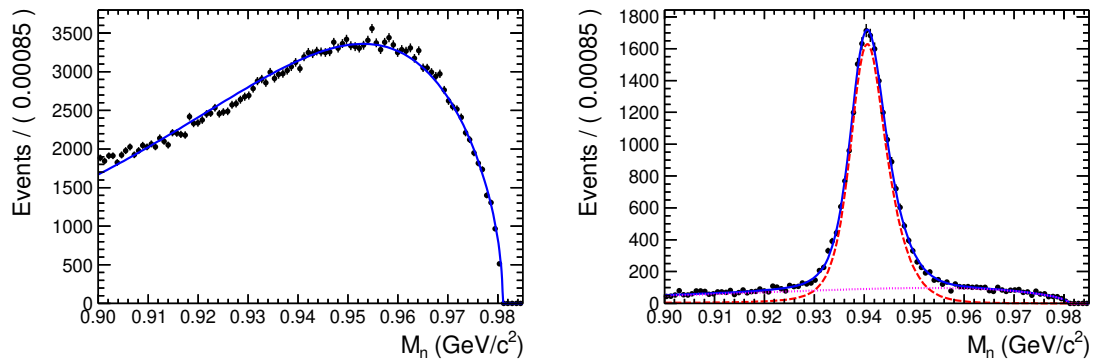


Figure 49: 2012 neutron channel